AGU ADVANCING EARTH AND SPACE SCIENCE

Abundance and Fractional Solubility of Aerosol Iron During Winter at a Coastal City in Northern China: Similarities and Contrasts Between Fine and Coarse Particles

Huanhuan Zhang[1,2,6], Rui Li[1,2], Shuwei Dong[1], Fu Wang[3], Yujiao Zhu[4] [ID], He Meng[5], Chengpeng Huang[3], Yan Ren[3], Xinfeng Wang[4], Xiaodong Hu[1], Tingting Li[1], Chao Peng[1], Guohua Zhang[1] [ID], Likun Xue[4] [ID], Xinming Wang[1] [ID], and Mingjin Tang[1,2,6] [ID]

[1]State Key Laboratory of Organic Geochemistry, Guangdong Key Laboratory of Environmental Protection and Resources Utilization, and Guangdong-Hong Kong-Macao Joint Laboratory for Environmental Pollution and Control, Guangzhou Institute of Geochemistry, Chinese Academy of Sciences, Guangzhou, China, [2]CAS Center for Excellence in Deep Earth Science, Guangzhou, China, [3]Longhua Center for Disease Control and Prevention of Shenzhen, Shenzhen, China, [4]Environment Research Institute, Shandong University, Qingdao, China, [5]Qingdao Eco-environment Monitoring Center of Shandong Province, Qingdao, China, [6]University of Chinese Academy of Sciences, Beijing, China

Abstract Aerosol deposition is a major source of soluble Fe in open oceans, affecting marine biogeochemistry and primary production. However, Fe fractional solubility, a key parameter in estimating deposition fluxes of soluble aerosol Fe, is still highly uncertain. Abundance and fractional solubility of aerosol Fe in fine (<1 μm) and coarse (>1 μm) particles was measured at Qingdao (a coastal city in northern China) in November-December 2019. Average concentrations of total and soluble Fe were found to be 798 ± 466 and 7.7 ± 14.5 ng/m^3 in coarse particles, and 801 ± 534 and 7.3 ± 7.6 ng/m^3 in fine particles. Fe solubility was significantly lower in coarse particles (average: $0.80 \pm 1.03\%$) than fine particles (average $1.29 \pm 1.41\%$). Compared to clean days, total Fe concentration was substantially increased during dust and haze days; however, Fe solubility was significantly reduced in dust days and elevated in haze days. Acid processing significantly enhanced Fe solubility in both fine and coarse particles, and the contribution of primary emission to Fe solubility enhancement was important for fine particles but minor for coarse particles. Higher Fe solubility ($>1\%$) in fine and coarse particles was usually observed at high aerosol acidity (pH < 4) and high RH ($>60\%$), suggesting critical roles of aerosol acidity and water content in regulating aerosol Fe solubility.

1. Introduction

Iron (Fe), an essential micronutrient for all the living organisms, plays important roles in photosynthesis, respiration and nitrogen fixation of marine phytoplankton (Moore et al., 2013). Although it is one of the most abundant elements in the crust, concentration of dissolved Fe in oceanic water is very low, limiting primary productivity and affecting phytoplankton ecosystem structures in many open oceans (Boyd & Ellwood, 2010; Jickells et al., 2005; Tagliabue et al., 2017). In high nutrient low chlorophyll (HNLC) regions (e.g., Southern Ocean, subarctic North Pacific and east tropical Pacific) which cover around 30% of global oceans, Fe supply directly limits or colimits photosynthesis and thus primary production (Jickells et al., 2014). Moreover, Fe supply limits or colimits microbial nitrogen fixation and thus also affects primary production over vast tropical nutrient-poor regions (e.g., tropical Pacific, South Atlantic, and Indian Ocean) (Jickells et al., 2014). There are evidence that increased supply of soluble Fe to some oceanic regions would increase primary productivity (Boyd et al., 2007; Tang et al., 2021), having important implications for CO$_2$ uptake and climate (Jickells et al., 2005). It has been proposed that increase in dust and thus Fe deposition during the last glacial maximum caused increase in carbon export to deep ocean and decrease in atmospheric CO$_2$ (Martin, 1990).

Major external sources of Fe in surface oceans include aerosol deposition, riverine input, continental margins, hydrothermal activities and glacial sediments, and aerosol deposition is a major Fe source for open oceans (Conway & John, 2014; Jickells et al., 2005; Tagliabue et al., 2017). In addition, aerosol Fe (as well as other transition metals such as Cu and Mn) also plays important roles in chemical reactivity of aerosol particles (Alexander et al., 2009; Martin & Good, 1991) and their health effects (Daellenbach et al., 2020; Fang et al., 2017). However, a large fraction of aerosol Fe may not be bioavailable. Fe availability is in fact poorly defined and understood, and soluble Fe has been widely used as a proxy for bioavailable Fe (Baker & Croot, 2010; Meskhidze et al., 2019).

Writing – review & editing: Guohua Zhang, Mingjin Tang

Desert dust was conventionally thought to be the major source for soluble aerosol Fe; however, a number of field measurements (Mahowald et al., 2018; Sholkovitz et al., 2012) found that Fe fractional solubility (defined as the ratio of soluble Fe to total Fe, often abbreviated as Fe solubility) of ambient aerosol particles was significantly higher than fresh desert dust (usually <0.5%) (Ito et al., 2021) and showed large spatial and temporal variability.

Aerosol Fe solubility was frequently observed to increase with decrease in total aerosol Fe (Baker & Jickells, 2006; Sholkovitz et al., 2012), and several mechanisms have been proposed to explain the observed variability of aerosol Fe solubility (Baker et al., 2021; Ito et al., 2019; Mahowald et al., 2018; Meskhidze et al., 2003). One mechanism is physical sorting (Baker & Jickells, 2006), that is, preferential deposition of coarser dust particles with lower Fe solubility leads to increase in relative contribution of finer particles with higher Fe solubility, though a later study (Shi, Woodhouse, et al., 2011) suggested that this effect was small. Atmospheric processing, including proton-promoted, ligand-promoted and reductive dissolution, could significantly increase aerosol Fe solubility, as suggested by laboratory (Chen & Grassian, 2013; Shi, Bonneville, et al., 2011; Wang et al., 2018), field (Li et al., 2017; Liu et al., 2021; Shi et al., 2020), and modeling work (Ito & Shi, 2016; Luo et al., 2005; Meskhidze et al., 2003; Myriokefalitakis et al., 2015; Scanza et al., 2018; Solmon et al., 2009). In addition, anthropogenic and pyrogenic aerosol Fe with higher solubility has also been proposed to explain the higher Fe solubility of ambient aerosol particles (when compared to fresh desert dust) (Chuang et al., 2005; Ito, 2015; Ito et al., 2019; Luo et al., 2008; Myriokefalitakis et al., 2015; Schroth et al., 2009; Sholkovitz et al., 2009). Despite many previous studies, it remains difficult to quantitatively explain and predict variability of Fe solubility of ambient aerosols, and contrasting results were also reported (for example, with respect to the effects of atmospheric processing) (Mahowald et al., 2018; Meskhidze et al., 2019). In fact, currently one major uncertainty in estimating deposition fluxes of soluble aerosol Fe to surface oceans stems from uncertainties in aerosol Fe solubility (Mahowald et al., 2018; Myriokefalitakis et al., 2018).

North Pacific is a major HNLC region where primary productivity is limited by Fe. The west part of North Pacific is affected by aerosol Fe from a myriad of sources in Asia, including desert dust, biomass burning, and anthropogenic emissions, providing a good place to investigate variability and controlling factors of aerosol Fe solubility. To further understand abundance and fractional solubility of aerosol Fe in this region, a field campaign was conducted in November-December 2019 at a suburban site in Qingdao, a coastal city in northern China. Compared to previous studies carried out over and around Northwest Pacific (Chuang et al., 2005; Fu, Shang, et al., 2014; Hsu et al., 2005, 2010; Liu et al., 2021; Ooki et al., 2009; Shi et al., 2020; Takahashi et al., 2013; Zhang et al., 2013; Zhu et al., 2020), our work aimed to provide further insights in the following three aspects: (a) fine (<1 μm) and coarse (>1 μm) particles were simultaneously collected. Fine and coarse particles exhibit large difference in sources and compositions (Seinfeld & Pandis, 2016), and therefore Fe solubility and its controlling factors may differ significantly between coarse and fine particles; (b) a number of elements and soluble ions, in addition to total and soluble Fe, were also measured, providing constrains to understand factors which determined aerosol Fe solubility; (c) three representative weather conditions, including clean, haze and dust days, were encountered during the campaign, giving the opportunities to explore and understand aerosol Fe solubility under distinctively different conditions.

2. Methodology

2.1. Sample Collection

Aerosol particles were collected at a rural/suburban site in Qingdao which is a coastal city in northern China between 07 November and 19 December 2019, except 23 November, 01 December, and 16 December due to technical failure. Qingdao has a total population of around 11 million and is affected by Asian outflow of desert dust and anthropogenic pollution. Aerosol sampling was conducted on the roof of a 5-floor building (36.34°N, 120.67°E) which is ~20 m above the ground level and ~1.3 km from the coastline. The sampling site is surrounded by a number of residence/office buildings, villages and farmlands, and two expressways are located to its west (~900 m) and north (~1,200 m) (Cui et al., 2021). A two-stage medium volume aerosol sampler (TH-150C, Tianhong Co.), which has a sampling flow rate of 100 L/min, was used to collect fine (<1 μm) and coarse (>1 μm) particles simultaneously, in an attempt to separate natural and anthropogenic aerosol particles to some extent (Seinfeld & Pandis, 2016). Aerosol sampling was started at 08:00 on each day and stopped at 07:30 on the next day, and in total 141 m³ air was sampled in 23.5 hr. After the sampling was stopped, filters were taken out from the aerosol sampler, placed into sealed plastic Petri dishes and stored frozen at −20°C in a fridge for later

analysis at Guangzhou Institute of Geochemistry, Chinese Academy of Sciences. Filters before and after aerosol collection were weighted using a high-precision balance (with a mass resolution of 1 μg) in a RH-controlled room (RH<50%) at around 20°C.

Whatman 41 (W41) cellulose filters were used in our work to collect aerosol particles due to its low background and high collection efficiency, as recommended by previous work (Morton et al., 2013). W41 cellulose filters, which were commercially available as rectangular sheets (254 × 203 mm), were cut in our lab to circular (88 mm in diameter) and annular filters (od: 74 mm; id: 21 mm) which were used to collected fine and coarse particles, respectively. Circular and annular filters were then pretreated using a protocol similar to that recommended by previous work (Morton et al., 2013) to minimize the background: (a) filters were soaked in 0.5 mol/L HCl for 24 hr and then soaked in deionized water (>18.2 MΩ cm^{-1}) for 24 hr; (b) they were rinsed three times in deionized water, and after the third rinsing the pH of the water bath reached 5.4–5.6; (c) these filters were dried in an oven at 50°C, individually placed into sealed plastic Petri dishes, and stored at −20°C in a fridge.

In addition, all the labwares in contact with or used to extract/digest filters were soaked in 0.5 mol/L HCl for 24 hr, rinsed three times with deionized water, and dried at 40°C in an oven for 12 hr. In our work, 36%–38% HCl (GR grade) was provided by Guangzhou Chemical Reagent Factory, and it was also used to prepare 0.5 mol/L HCl; unless otherwise stated, HNO_3 (Optima Grade, Fisher Scientific) was used as received (67%–70%) or diluted to 1% HNO_3 solution.

Meteorological (temperature, relative humidity, and wind speed and direction) and air quality (mass concentrations of $PM_{2.5}$ and PM_{10}) data were obtained from an adjacent air quality monitoring station operated by Qingdao Eco-environment Monitoring Center. In addition, black carbon (BC) was measured using an aethalometer (AE33, Magee Scientific Co.).

2.2. Sample Analysis

2.2.1. Measurements of Soluble Ions and Metals

Each particle-loaded filter was divided into two equivalent halves using a ceramic knife. The first half was extracted in 20 mL deionized water for 2 hr, continuously stirred using an orbital shaker (300 r/min). The extraction was immediately filtered through a 0.22 μm PTFE membrane syringe filter and then divided to two parts. The first part (∼10 mL) was analyzed using ion chromatography (761 Compact IC, Metrohm) to measure concentrations of soluble anions (NO_3^-, SO_4^{2-}, Cl^-, NO_2^- and oxalate) and cations (NH_4^+, Na^+, K^+, Ca^{2+}, and Mg^{2+}) (Fu, Wang, et al., 2014; Fu et al., 2015). Detection limits were estimated to be 10–20 μg/L in the solution and 3–6 ng/m^3 in the air for soluble ions. Background levels of blank filters were around or below 10–20, 30–50, and 70–80 ng/m^3 for NO_3^-, Cl^-, and NH_4^+, and below detection limits for the other seven ions. We found that background levels of NO_3^-, Cl^-, and NH_4^+ were significantly lower for freshly prepared filters and would increase during storage, as cellulose filters could adsorb HCl, HNO_3, and NH_3 from ambient air (Morton et al., 2013).

The second part of the solution (10 mL) was acidified with 147 μL HNO_3 (67%–70%) to contain 1% HNO_3 and then analyzed using inductively coupled plasma mass spectrometry (ICP-MS, iCAP Q, Thermo Fisher Scientific) to determine concentrations of metals. In total, 14 metals were analyzed, and inner standards used were Sc (for Al), Ge (for Cr, Cu, Fe, Mn, Ni, V, and Zn), Y (for As and Se), In (for Cd), and Bi (for Ba, Pb, and Sb). Three measurements were carried out for each solution (both soluble and total metals) to report the average value. Detection limits in the solution were estimated to be around 1 μg/L for Fe, Ba, and Zn and around 0.1 μg/L for other metals, corresponding to 0.3 and 0.03 ng/m^3 in the air. Soluble metals were always below their detection limits for blank filters. As summarized by Meskhidze et al. (2019), a variety of leaching solutions have been used to extract soluble aerosol Fe, likely leading to considerable difference in results obtained, and the community is yet to reach consensuses in leaching methods. We chose to use deionized water which was widely used in previous work to extract soluble aerosol Fe.

2.2.2. Measurements of Total Metals

Teflon jars used in digestion were washed using the following procedure to minimize the background: (a) each Teflon jar was first washed four times with deionized water and dried at 100°C in an oven; (b) it was filled with 2 mL deionized water and 4 mL HCl (36%–38%), and was then kept at 180°C in a microwave digestion instrument for 1 hr (it should be mentioned that Teflon jars were always tightly capped during microwave digestion);

(c) the Teflon jar was washed three times with deionized water after residual acids were removed, filled with 2 mL deionized water and 4 mL 65%–68% HNO_3 (GR grade, Guangzhou Chemical Reagent Factory), and then kept at 180°C in a microwave digestion instrument for 1 hr; (d) it was washed three times with deionized water after residual acids were removed, filled with 1 mL deionized water and 3 mL HNO_3 (67%–70%), and then kept at 180°C in a microwave digestion system for 1 hr; (e) finally, the Teflon jar was washed three times with deionized water after residual acids were removed, and then dried at 100°C in an oven.

To digest the second half of a particle-loaded filter, it was shredded using ceramic scissors and transferred into a pre-cleaned Teflon jar. It should be mentioned that in some cases only one quarters of a filter was used in digestion. The following procedure was adopted in our work to digest the filter sample: (a) The Teflon jar was filled with 2 mL HNO_3 (67%–70%) and 2.5 mL H_2O_2 (31%, G5, ICPMS Pure grade, Aoban Technology Company Limited, Shanghai, China), and then kept at room temperature in a fume hood for 24 hr; (b) after that, it was filled with 3 mL HNO_3 (67%–70%) and 1 mL HF (47%–51%, Optima grade, Fisher Scientific) and kept at 170°C in a microwave digestion instrument for 2 hr (please note that the filter/HNO_3/H_2O_2 mixture was not dried before HNO_3 and HF was added into the Teflon jar); (c) the Teflon jar was transferred onto a heating plate and heated at 140°C for ~4 hr to evaporate residual acids; (d) after it was cooled down to room temperature, the Teflon jar was filled with 20 mL 1% HNO_3, and the solution was filtered through a 0.22 μm PTFE membrane syringe filter. The filtration was analyzed by ICP-MS to determine total metal concentrations. Two certificated reference materials (GBW07454, provided by Chinese Academy of Geological Sciences; GSB07-3272-2015, provided by Institute for Environmental Reference Materials, Ministry of Environmental Protection) were used in our work to check digestion recoveries, which were found to be 104%–114% for Fe, 115%–119% for Al, 83%–131% for Pb, 100%–110% for V, and 83%–95% for Ni. In our work, background levels in blank filter were found to be <5, <20, <5, and <10 ng/m^3 for total Fe, Al, Ba and Zn, 1–2 ng/m^3 for total Cr and Cu, and <0.5 ng/m^3 for other metals.

2.3. Aerosol Acidity Calculation

The measured concentrations of water soluble inorganic ions and daily averaged temperature and RH (relative humidity) were used as input in the aerosol thermodynamic model ISORROPIA-II (Fountoukis & Nenes, 2007) to calculate aerosol liquid water content and pH for fine and coarse particles. We did not take into account organics, and their influence on aerosol liquid water content and pH was estimated to be small in China (Liu et al., 2017). The model was run in the forward mode and aerosol particles were assumed to be metastable, as previous work (Guo et al., 2015; Hennigan et al., 2015) found that the forward mode gave better estimation of aerosol pH than the reverse mode when only aerosol composition data was available. In our calculations NH_3 and HNO_3 in the gas phase were implicitly assumed to be negligible when compared to NH_4^+ and NO_3^- in aerosol particles, and this would lead to uncertainties in calculated aerosol acidity. The same method was also used in a recent study (Wang et al., 2021) to calculate aerosol pH for PM$_{2.5}$ samples in Shanghai. We also tried to use the iteration process (Fang et al., 2017) to calculate aerosol pH, but the results failed to converge.

3. Results

3.1. Overview of Meteorological Conditions and Aerosol Pollution

Figure 1 shows time series of wind speed and direction, temperature and RH, and mass concentrations of PM$_{2.5}$ and PM$_{10}$ during the campaign. Wind mainly came from northwest, and its speeds typically ranged from 2 to 6 m/s (Figure S1); when wind came from other directions (mainly south), its speeds were usually <4 m/s. Over the entire campaign temperature was in the range of −7°C to 21°C with a median value of 5°C, and RH was in the range of 34%–94% with a median value of 66%.

Three representative weather conditions, including dust, haze and clean days, were identified based on mass concentrations of PM$_{2.5}$ and PM$_{10}$. Three days (18–20 November) were classified as dust days: wind mainly came from northwest and was usually above 2 m/s, PM$_{10}$ exceeded 100 μg/m^3, and mass concentration ratios of PM$_{10}$ to PM$_{2.5}$ reached 3. Four days (07–10 December) were classified as haze days during which air was stagnant (wind speed <2 m/s) and average RH was >70%, accomplished by significant increase in BC and secondary inorganic species (Figure S2). During the seven clean days (22–25 November and 15–17 December) mass concentrations of PM$_{2.5}$ and PM$_{10}$ were both below 50 μg/m^3. In addition, no obvious fogs occurred during our campaign.
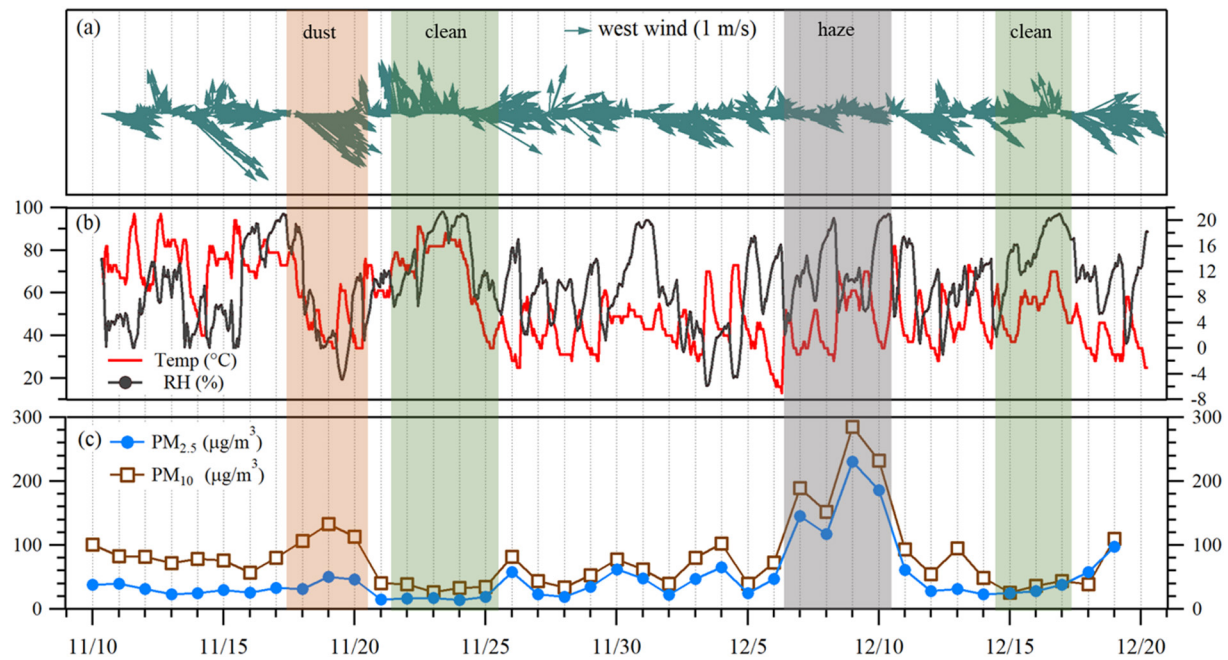
Figure 1. Time series of (a) wind speed and direction, (b) temperature and RH, and (c) mass concentrations of $PM_{2.5}$ and PM_{10}.

3.2. Total and Soluble Aerosol Iron

3.2.1. Total Aerosol Fe

Figure 2 displays time series of mass concentrations of total Fe, mass fractions of total Fe (normalized to particle mass concentrations), mass concentrations of soluble Fe, and Fe solubility for fine and coarse particles. As shown
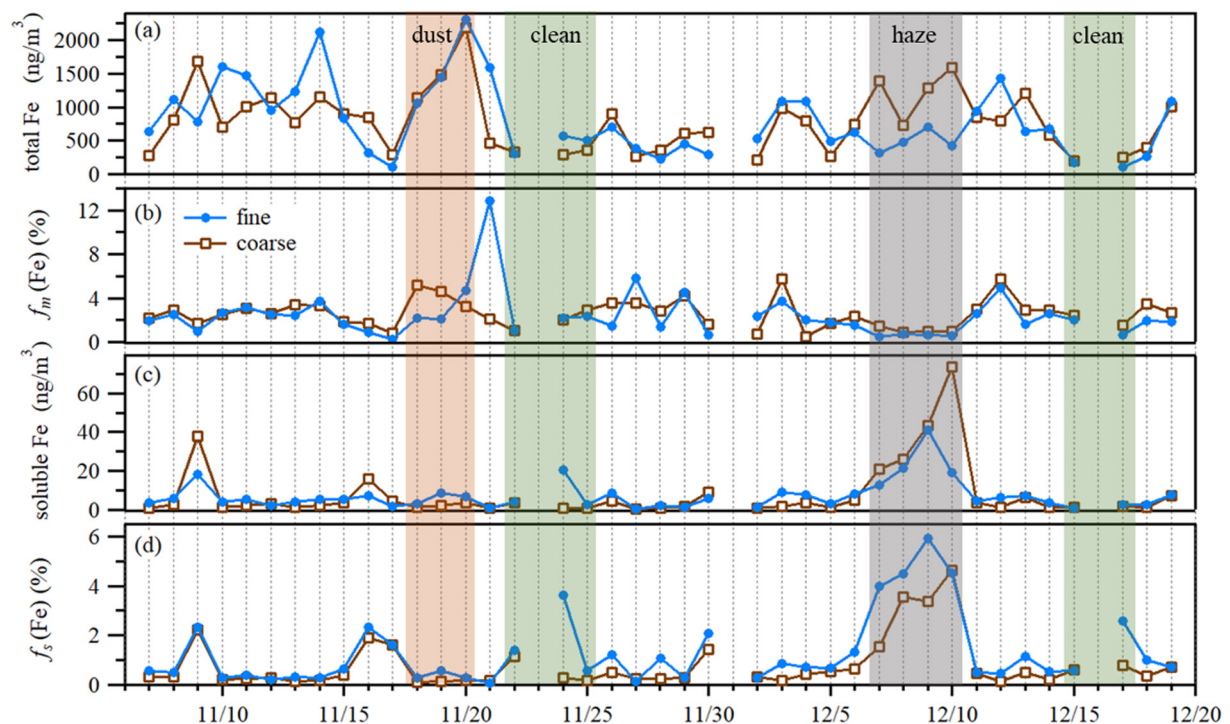

Figure 2. Time series of (a) total Fe, (b) mass fraction of Fe, (c) soluble Fe, and (d) Fe fractional solubility in fine and coarse particles.

Table 1
Overview of Total Fe (in ng/m³), Mass Fractions of Fe (f_m(Fe), in %), Soluble Fe (in ng/m³) and Fe Fractional Solubility (f_s(Fe), in %) in Fine and Coarse Particles During the Campaign

	Fine particles			Coarse particles		
	Range	Average	Median	Range	Average	Median
Total Fe	104–2,301	801 ± 534	654	195–2,193	798 ± 466	780
f_m(Fe)	0.28–12.84	2.40 ± 2.13	2.04	0.48–5.75	2.58 ± 1.31	2.55
Soluble Fe	0.6–41.2	7.3 ± 7.6	5.6	0.6–73.7	7.7 ± 14.5	2.3
f_s(Fe)	0.07–5.91	1.29 ± 1.41	0.66	0.11–4.63	0.80 ± 1.03	0.34

in Table 1, mass concentrations of aerosol Fe were in the range of 195–2,193 ng/m³ for coarse particles (average: 798 ± 466 ng/m³; median: 780 ng/m³) and 104–2,301 ng/m³ for fine particles (average: 801 ± 534 ng/m³; median: 654 ng/m³). No significant difference in aerosol Fe concentrations was found between fine and coarse particles (paired t-test, $P = 0.96$, $\alpha = 0.05$). Figure 3a compares mass concentrations of aerosol Fe under different weather conditions. Average mass concentrations of aerosol Fe were determined to be 1,605 ± 538 and 1,601 ± 635 ng/m³ for coarse and fine particles during dust days, 1,252 ± 367 and 480 ± 160 ng/m³ during haze days, and 285 ± 63
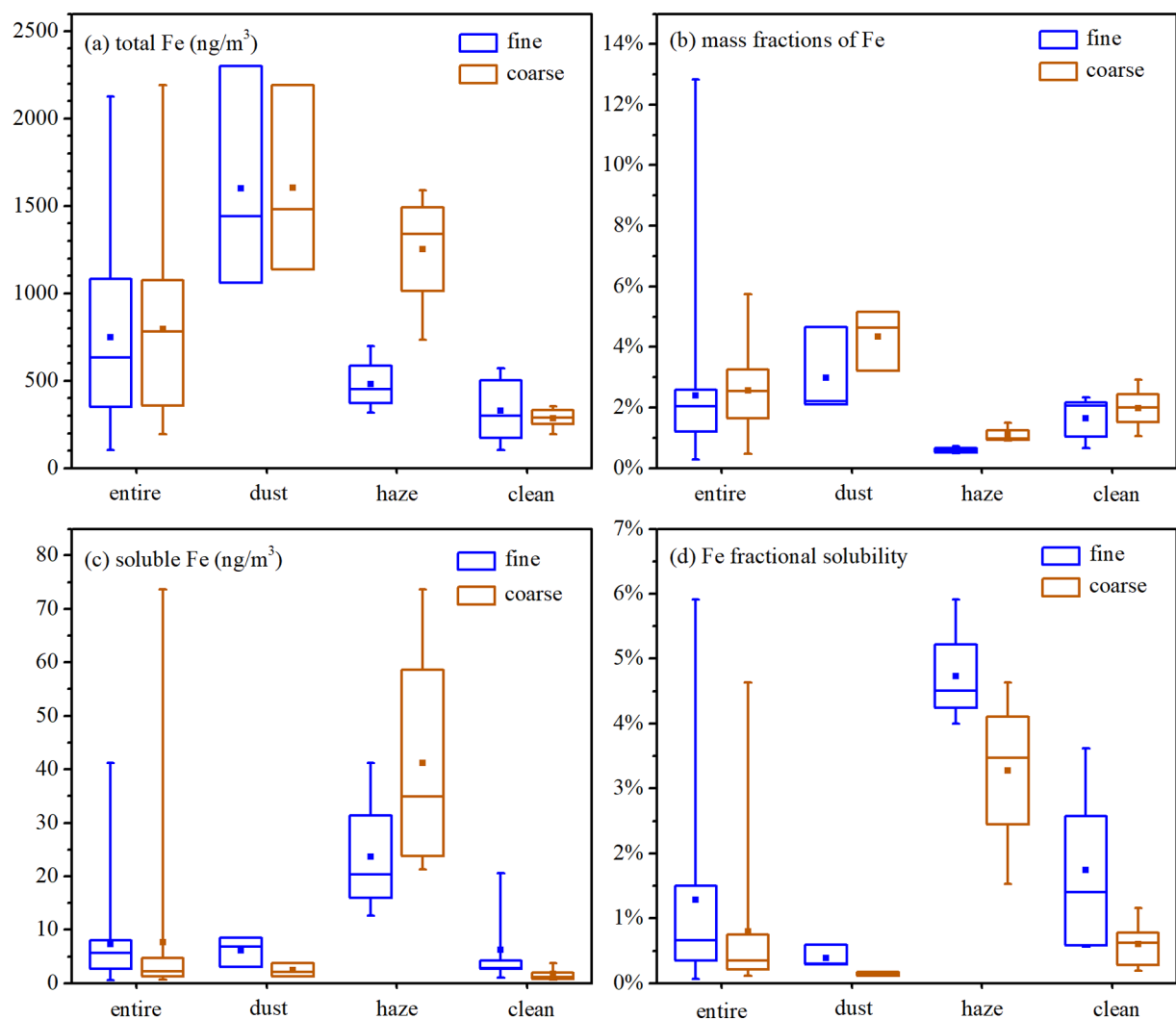

Figure 3. Total Fe (a), mass fractions of Fe (b), soluble Fe (c), and Fe solubility (d) in fine and coarse particles under different weather conditions.
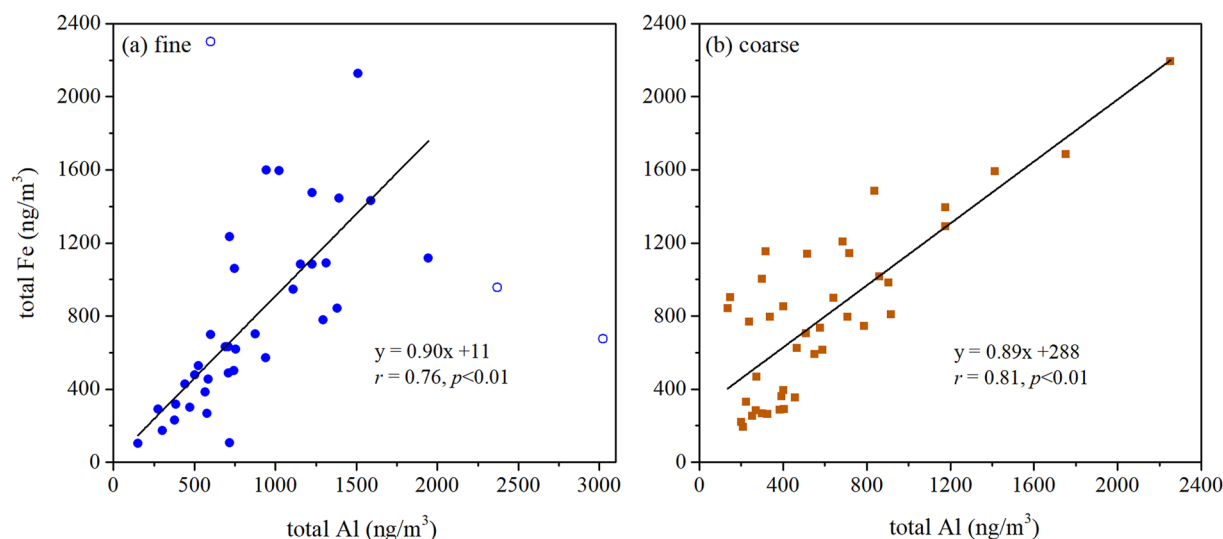
Figure 4. Total Fe versus total Al in fine (a) and coarse (b) particles. Data represented by the three open circles in Figure 4a are excluded from correlation analysis.

and 329 ± 203 ng/m^3 during clean days. This suggests that both dust and anthropogenic emission could substantially increase total Fe concentrations in fine and coarse particles. Total Fe concentrations in total suspended particles (TSP) were measured to be 2.2–4.5 µg/m^3 during dust days in our work, significantly lower than those (median: 15 µg/m^3) found during dust episodes in 2013 at the same city (Shi et al., 2020), and the difference was due to different intensities of dust events observed in the two studies.

The range, average and median values were determined to be 0.48%–5.75%, $2.58 \pm 1.31\%$ and 2.55% for mass fractions of total Fe in coarse particles, and 0.28%–12.84%, $2.40 \pm 2.13\%$ and 2.04% in fine particles (Table 1). There was no significant difference in mass fractions of total Fe between fine and coarse particles (paired t-test, $P = 0.59$, $\alpha = 0.05$). As shown in Figure 3b, average mass fractions of total Fe were found to be $5.16 \pm 4.64\%$ and $2.99 \pm 1.44\%$ for coarse and fine particles during dust days, $1.09 \pm 0.27\%$ and $0.60 \pm 0.10\%$ during haze days, and $1.99 \pm 0.73\%$ and $1.65 \pm 0.75\%$ during clean days. Mass fractions of aerosol Fe during dust days were similar to those (around 3.5% but quite variable) reported for the upper continental crust (Taylor & McLennan, 1995) and desert dust in source regions (Cao et al., 2008; Zhang et al., 2014), significantly higher than clean days; in addition, during dust days mass fractions of Fe was higher in coarse particles than fine particles, because desert dust was mainly present in coarse particles. In contrast, compared to clean days, Fe mass fractions were significantly reduced during haze days (especially for fine particles), due to large increase in secondary species during haze events.

Total Fe is well correlated with total Al for both fine and coarse particles (Figure 4), suggesting desert dust as the major source for aerosol Fe in fine and coarse particles. Median values of Fe/Al mass ratios were found to be 1.123 for coarse particles and 0.825 for fine particles. Using the mass ratio of Fe/Al in the upper continental crust as the reference (0.435) (McLennan, 2001; Taylor & McLennan, 1995), median values of Fe enrichment factors were determined to be 2.6 and 1.9 for coarse and fine particles. It has been suggested that Fe enrichment factor of >1.3 implies existence of non-crustal sources for aerosol Fe (Mahowald et al., 2005; Wiersma & Davidson, 1986); as a result, nondust sources were not negligible for aerosol Fe observed in our work.

3.2.2. Soluble Aerosol Fe

During our campaign, the range and average and median values were found to be 0.6–73.7, 7.7 ± 14.5, and 2.3 ng/m^3 for soluble Fe concentrations in coarse particles, and 0.6–41.2, 7.3 ± 7.6, and 5.6 ng/m^3 in fine particles (Table 1). The difference in soluble Fe concentrations was not statistically significant between coarse and fine particles (paired t-test, $P = 0.81$, $\alpha = 0.05$).

Significant difference in soluble Fe concentrations was observed under different weather conditions. As shown in Figure 3c, average soluble Fe concentrations were found to be 2.4 ± 1.3 and 6.1 ± 2.8 ng/m^3 for coarse and fine particles during dust days, 41.2 ± 23.7 and 23.7 ± 12.3 ng/m^3 during haze days, and 1.7 ± 1.3 and 6.3 ± 8.1 ng/m^3

during clean days. Compared to haze days, during dust days total Fe concentrations were higher but soluble Fe concentrations were much lower. Such contrast was caused by difference in Fe solubility under the two weather conditions, and will be further discussed in Section 3.3.

We further examined correlation between soluble Fe and a few source tracers, including total Al, total Pb, BC and nss-K$^+$ (non-sea-salt K$^+$). Mass concentrations of nss-K$^+$ and nss-sulfate (non-sea-salt sulfate) can be calculated using Equation 1:

$$[\text{nss-X}] = [\text{X}] - \alpha_{\text{X}} \cdot [\text{Na}^+] \tag{1}$$

where X is sulfate or K$^+$, [Na$^+$] is the mass concentration of soluble Na$^+$, and α_{X} is equal to 0.252 for sulfate and 0.036 for K$^+$ (Piel et al., 2006). As shown in Figure 5, soluble Fe was well correlated with total Al, total Pb, BC, and nss-K$^+$ for coarse particles, indicating that both desert dust as well as combustion and anthropogenic sources contributed to soluble Fe in coarse particles. On the contrary, soluble Fe was well correlated with total Pb, BC, and nss-K$^+$ but not with total Al for fine particles, implying that contribution of desert dust to soluble Fe in fine particles might be small.

3.3. Aerosol Fe Solubility

The range, average and median values of Fe solubility were found to be 0.11%–4.63%, 0.80 ± 1.03% and 0.34% for coarse particles, and 0.07%–5.91%, 1.29 ± 1.41%, and 0.66% for fine particles. During our campaign Fe solubility was significantly higher in fine particles than coarse particles (paired t-test, $P < 0.05$, $\alpha = 0.05$). Increase in Fe solubility with decrease in particle size has been observed at various locations around the globe by previous work (Baker et al., 2006b, 2020; Chen & Siefert, 2004; Fang et al., 2017; Gao et al., 2019, 2020; Johansen & Hoffmann, 2003; Longo et al., 2016; Ooki et al., 2009; Siefert et al., 1999), despite that different leaching protocols were employed to extract soluble Fe from collected ambient aerosol particles. Therefore, increase in Fe solubility with decrease in particle size may be a universal phenomenon, though one previous study (Buck, Landing, & Resing, 2010) found that Fe solubility did not increase with decreasing particle size for aerosol particles collected over the North Atlantic Ocean in June–August 2003.

Size-dependence of aerosol Fe solubility could be caused by two reasons. First of all, dust particles with lower Fe solubility are mainly present in coarse particles, while anthropogenic particles with higher Fe solubility are enriched in fine particles. In addition, aerosol acidity is typically higher in fine particles than coarse particles (Kakavas et al., 2021), and thus enhancement of Fe solubility by acid processing can be more significant for fine particles. This is supported by the fact that over the entire campaign calculated pH values were significantly lower (paired t-test, $P < 0.01$, $\alpha = 0.05$) for fine particles (average: 3.64 ± 0.77; median: 3.68) than coarse particles (average: 4.24 ± 1.17; median: 3.99).

A number of previous studies (Baker & Jickells, 2006; Gao et al., 2013; Hsu et al., 2005, 2010; Kumar & Sarin, 2010; Kumar et al., 2010; Mahowald et al., 2018; Meskhidze et al., 2019; Sedwick et al., 2007; Shelley et al., 2018; Sholkovitz et al., 2012; Winton et al., 2015) have revealed the inverse dependence of Fe solubility on total aerosol Fe concentration (or mass concentration of dust aerosol), despite that these studies used various leaching methods to determine Fe solubility. Several mechanisms, including physical sorting (Baker & Jickells, 2006), anthropogenic and pyrogenic aerosol Fe (Sholkovitz et al., 2009), and chemical processing (Meskhidze et al., 2003), can explain the observed inverse dependence, though quantitative understanding has not been reached. Similar to these studies, an inverse relation was observed in our work between Fe solubility and total Fe concentration (and total Al concentration as well) for fine particles, as shown in Figure 6a; however, such an inverse dependence was not observed for coarse particles (Figure 6b). We notice that two previous studies (Oakes, Weber, et al., 2012; Paris et al., 2010) also reported no obvious dependence of Fe solubility on total Fe mass concentration, and aerosol particles were collected over the West African Sahel (Paris et al., 2010) and in Atlanta, Georgia, USA (Oakes, Weber, et al., 2012).

Figure 3d reveals significant difference in Fe solubility for the three representative weather conditions. Average Fe solubility was 0.14 ± 0.03% and 0.39 ± 0.17% for coarse and fine particles during dust days, much lower than those during clean days (0.61 ± 0.39% and 1.75 ± 1.33% for coarse and fine particles). Fe solubility was usually <1% for dust particles collected from topsoil in source regions (Oakes, Ingall, et al., 2012; Paris & Desboeufs, 2013; Paris et al., 2011; Shi, Woodhouse, et al., 2011) and dust aerosols collected over the West African
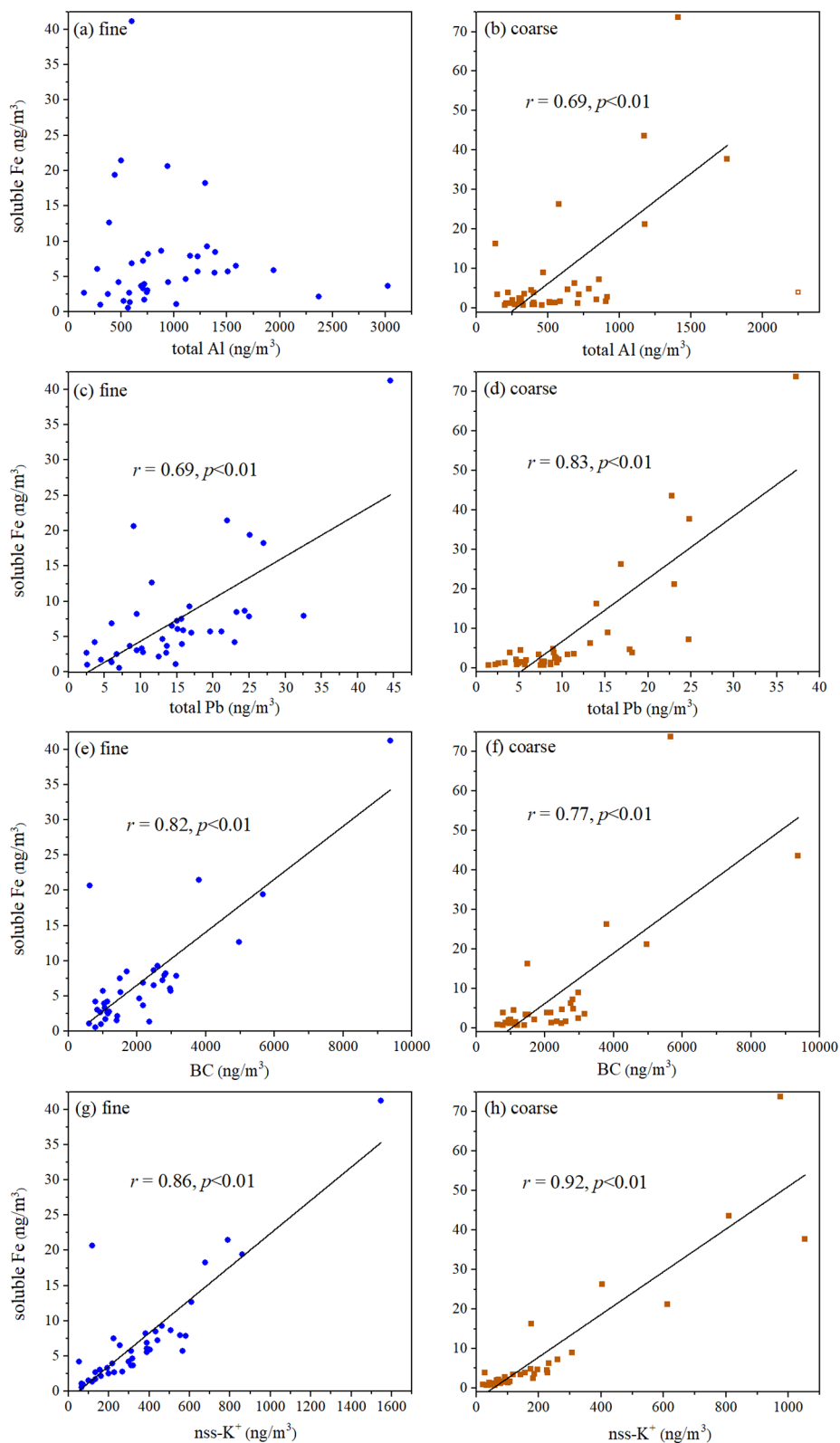
Figure 5. Soluble Fe versus total Al (a), total Pb (c), BC (e), and nss-K$^+$ (g) for fine particles; soluble Fe versus total Al (b), total Pb (d), BC (f), and nss-K$^+$ (h) for coarse particles.
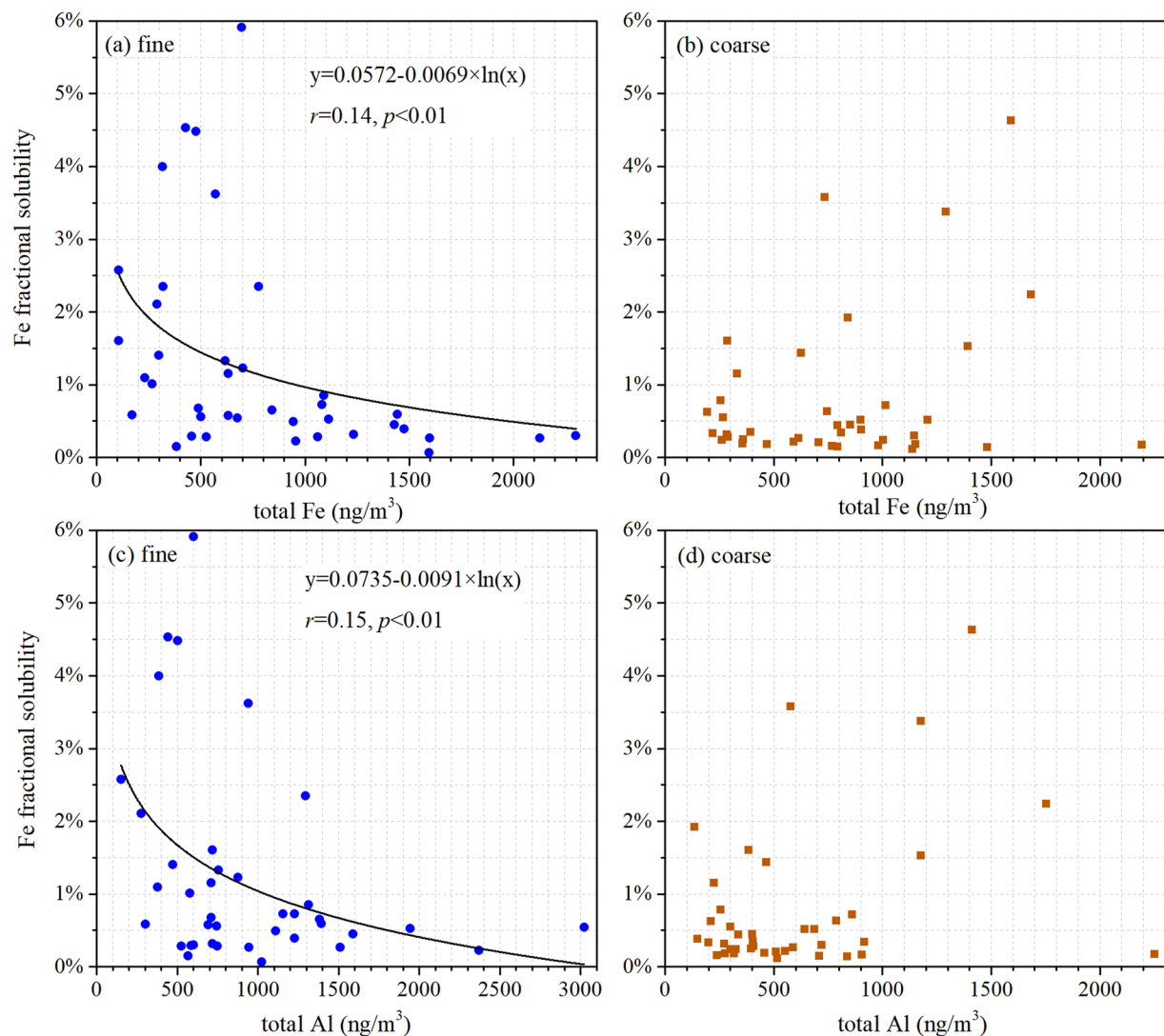
Figure 6. (a) Fe solubility versus total Fe for fine particles; (b) Fe solubility versus total Fe for coarse particles; (c) Fe solubility versus total Al for fine particles; (d) Fe solubility versus total Al for coarse particles.

Sahel (Paris et al., 2010), very similar to that for aerosol particles collected in our work during dust days at Qingdao, implying that Fe solubility was not significantly enhanced when desert dust aerosol was transported to Qingdao. This is supported by previous field measurements (Chuang et al., 2005; Fu, Shang, et al., 2014; Ooki et al., 2009; Shi et al., 2020). For example, during dust events Fe solubility observed at Jeju Island (Korea) was not significantly higher than that observed at Dunhuang (China) which is close to a major desert (Chuang et al., 2005); Fe solubility of large mineral dust particles (4.7–11 μm) transported to Hokkaido (northern Japan) was determined to be 0.52% (Ooki et al., 2009), very closed to 0.33% for an Asian dust standard. Similarly, average Fe solubility during dust days was determined to be $0.5 \pm 0.1\%$ for $PM_{2.5}$ samples in Shanghai (a coastal site in southeast China) (Fu, Shang, et al., 2014) and 0.27% for TSP in Qingdao (Shi et al., 2020).

Compared to clean days, Fe solubility was substantially enhanced during haze events, being $3.28 \pm 1.29\%$ for coarse particles and $4.73 \pm 0.82\%$ for fine particles on average. Significant increase in Fe solubility during haze days, when compared to clear days, was also observed by previous work (Shi et al., 2020; Zhu et al., 2020). This phenomenon was usually attributed to either increased contribution of anthropogenic particles with higher Fe solubility (Shi et al., 2020) or enhancement of aerosol Fe solubility due to chemical processing in haze days (Zhu et al., 2020). However, their contributions cannot be clearly distinguished or quantified yet. The median Fe

solubility for TSP was measured to be 5.81% during fog days and 1.75% during haze days in Qingdao by a previous study (Shi et al., 2020), higher and lower than those observed during haze days in our work.

4. Discussion

4.1. Effects of Anthropogenic Emission on Fe Solubility

Many field (Chuang et al., 2005; Conway et al., 2019; Guieu et al., 2005; Sedwick et al., 2007; Sholkovitz et al., 2012) and modeling studies (Ito, 2013; Ito & Shi, 2016; Ito et al., 2019, 2021; Luo et al., 2008; Mahowald et al., 2018) suggested that anthropogenic and combustion Fe would contribute significantly to soluble aerosol Fe in many regions and could at least in part explain higher Fe solubility (compared to that for fresh mineral dust) observed at various locations. For example, soluble aerosol Fe was not correlated with sulfate but with BC, indicating large contribution of combustion emission to observed high levels of aerosol soluble Fe (Chuang et al., 2005); in addition, Fe solubility was found to be correlated with Fe/Al, Pb/Al, and Cd/Al (Kumar & Sarin, 2010) and V/Al (Sholkovitz et al., 2009), indicating significant impacts of anthropogenic emission on aerosol Fe solubility.

Here we attempted to seek the dependence of measured Fe solubility on the abundance of three tracers, including BC which is dominantly emitted by combustion, nss-K^+ which is used as a tracer for biomass burning, and Pb which is used as a tracer for vehicle exhaust, coal combustion and metallurgical industry (Pant & Harrison, 2012; Viana et al., 2008). The molar ratios of nss-K^+ and Pb to Al, which are proportional to enrichment factors, were used in our work. As shown in Figure 7, Fe solubility was positively correlated with [BC], [nss-K^+]/[Al] and [Pb]/[Al] for fine particles, indicating that anthropogenic and combustion emissions could contribute significantly to enhanced Fe solubility of fine particles. Fe solubility was also positively correlated with [BC] and [nss-K^+]/[Al] for coarse particles, though these correlations were worse than fine particles; nevertheless, it was not significantly correlated with [Pb]/[Al]. If we do not include outliers in our analysis, as shown in Figure S7, Fe solubility was not correlated with [BC] or [Pb]/[Al] and only weakly correlated with [nss-K^+]/[Al] for coarse particles. Therefore, the contribution of anthropogenic and combustion emissions to enhanced Fe solubility might be minor for coarse particles, and the likely reason is that anthropogenic and pyrogenic Fe is mainly presented in fine particles.

Figure 7 further shows that both higher [BC], [nss-K^+]/[Al] and [Pb]/[Al] and higher Fe solubility were observed on haze days, suggesting that anthropogenic emission of aerosol Fe with higher solubility contributed to observed higher Fe solubility during haze days.

4.2. Effect of Acid Processing on Fe Solubility

It has been suggested that proton-promoted dissolution (i.e., acid processing) could substantially enhance aerosol Fe solubility (Baker et al., 2021; Chen & Grassian, 2013; Cwiertny et al., 2008; Ito & Feng, 2010; Li et al., 2017; Meskhidze et al., 2003; Scanza et al., 2018; Shi et al., 2012, 2015). Molar ratios of acidic species to total Fe were widely used in previous work (Liu et al., 2021; Shi et al., 2020; Zhu et al., 2020) to represent the relative degree of acid processing of aerosol Fe, and this method was also adopted in our work. We found that Fe solubility was well correlated with $(2 \times [SO_4^{2-}] + [NO_3^-])/[Fe]$ (Figure 8) as well as $[NO_3^-]/[Fe]$ and $[SO_4^{2-}]/[Fe]$ (Figure S3) for both fine and coarse particles, indicating that acid processing significantly enhanced Fe solubility in fine and coarse particles. It should be noted that in these two figures nss-sulfate, instead of total soluble sulfate, was used. As further shown in Figures 8 and S3, correlations between Fe solubility and acidic species (after normalized to total Fe) were always better for coarse particles; in contrast, correlations between Fe solubility with combustion tracers were always better for fine particles (Section 4.1). It is also apparent from Figure 8 that higher degrees of acid processing occurred during haze days (corresponding to higher Fe solubility) and lower degrees of acid processing was observed during dust days (corresponding to lower Fe solubility). It is worth mentioning that we only have four samples for haze days and three samples for dust days, and larger sample numbers are required to better understand the effects of anthropogenic emission and chemical processing on the enhancement of Fe solubility.

Many previous field studies investigated the relationship between Fe solubility and the abundance of acidic species, and contrasting results were reported. While Fe solubility was found to increase with acidic species in some studies (Kumar et al., 2010; Liu et al., 2021; Shi et al., 2020; Zhu et al., 2020), many other studies (Baker et al., 2006a, 2006b; Buck et al., 2006; Buck, Landing, Resing, & Measures, 2010; Chuang et al., 2005; Fu, Shang, et al., 2014; Ingall et al., 2018; Kumar & Sarin, 2010) did not observe such relationship. Nevertheless,
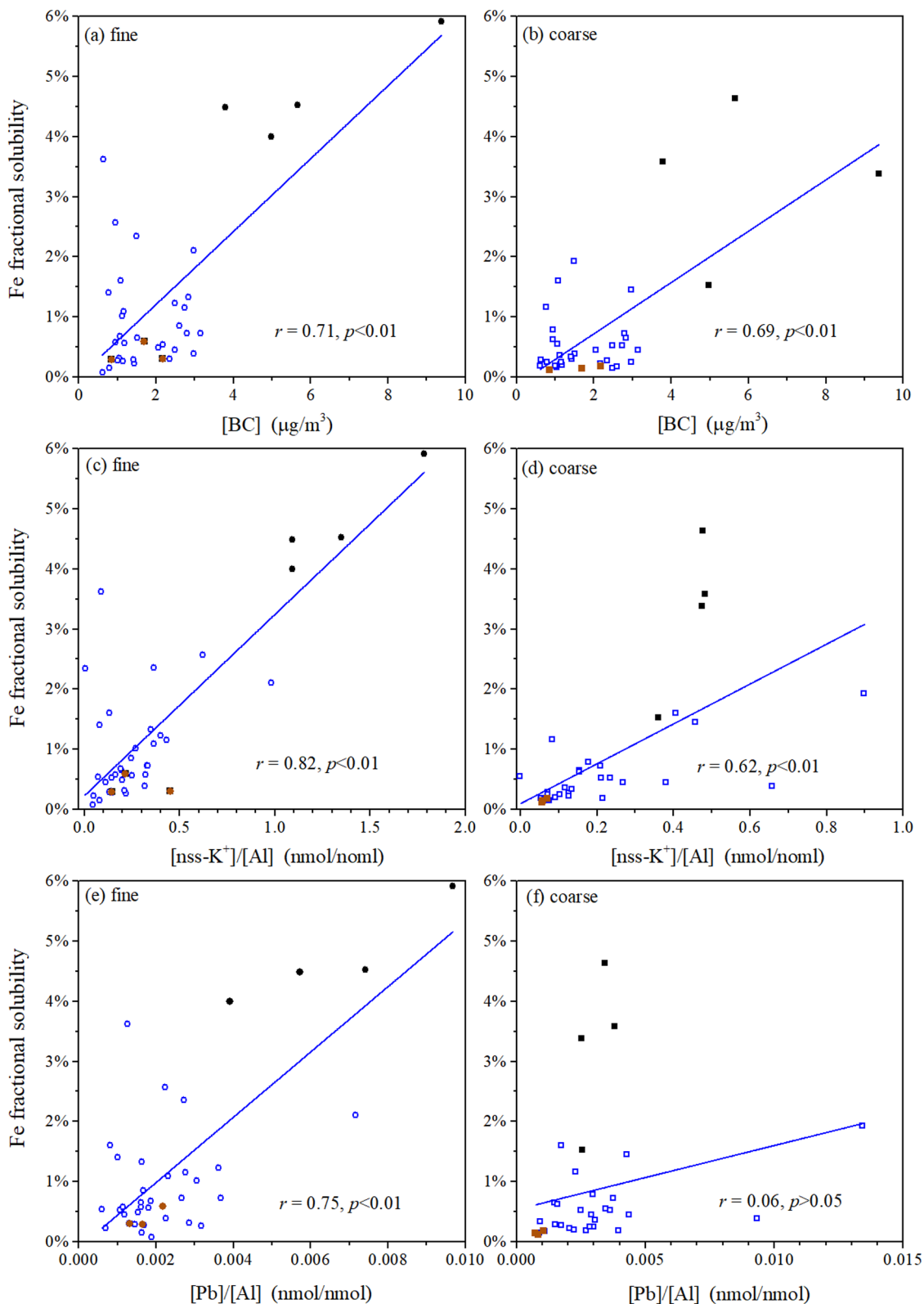
Figure 7. (a) Fe solubility versus BC concentrations for fine particles; (b) Fe solubility versus BC concentrations for coarse particles; (c) Fe solubility versus [nss-K$^+$]/[Al] for fine particles; (d) Fe solubility versus [nss-K$^+$]/[Al] for coarse particles; (e) Fe solubility versus [Pb]/[Al] for fine particles; (f) Fe solubility versus [Pb]/[Al] for coarse particles. Dust days are represented by solid brown symbols, and haze days are represented by solid black symbols.
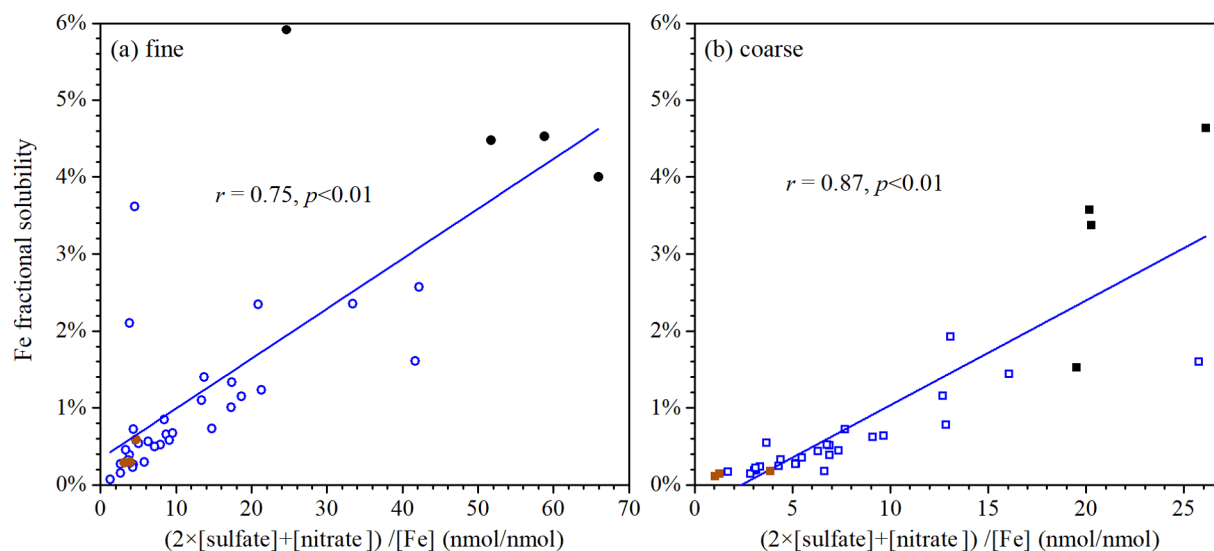
Figure 8. Fe solubility versus $(2 \times [\text{sulfate}] + [\text{nitrate}])/[\text{Fe}]$: (a) fine particles; (b) coarse particles. Dust days are represented by solid brown symbols, and haze days are represented by solid black symbols.

lack of such relationship does not necessarily mean that acid processing did not play an important role, because secondary acidic species (mainly sulfate and nitrate) would enhance Fe solubility, while their concentrations would decrease with time due to dispersion and deposition (Mahowald et al., 2018). As a result, it is more suitable to use relative abundance of acidic species (normalized to total Fe), instead of absolute abundance, to represent the degree of acid processing of aerosol Fe, as done in our work and some previous studies (Liu et al., 2021; Shi et al., 2020; Zhu et al., 2020). In fact, our work found that correlations of Fe solubility with absolute abundance of acidic species (Figures S4 and S5) were significantly worse than those with their relative abundance.

To further examine the impacts of proton-promoted dissolution on aerosol Fe solubility, we calculated aerosol pH using ISORROPIA-II, and Figure 9 plots Fe solubility versus calculated aerosol pH for fine and coarse particles. When aerosol pH exceeded 4, Fe solubility was <1% for both fine and coarse particles, except one fine particle sample. A few previous studies (Fang et al., 2017; Ingall et al., 2018; Longo et al., 2016) also revealed the importance of aerosol acidity in Fe solubility. For example, increase in transport time led to increase in aerosol acidity
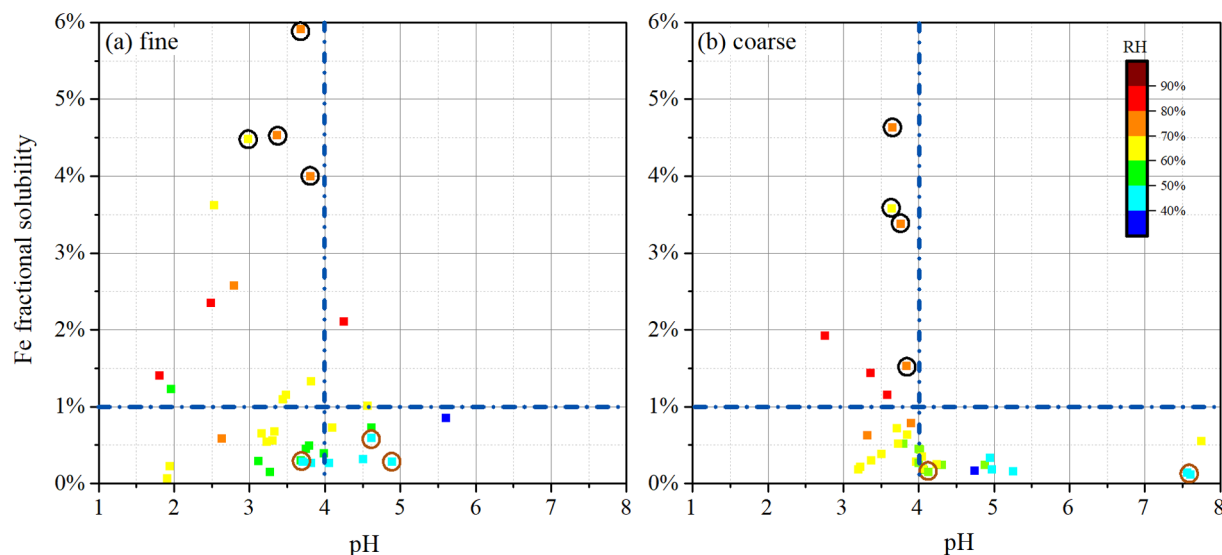

Figure 9. Fe solubility versus calculated aerosol pH: (a) fine particles; (b) coarse particles. Dust days are labeled using brown circles, and haze days are labeled with black circles.
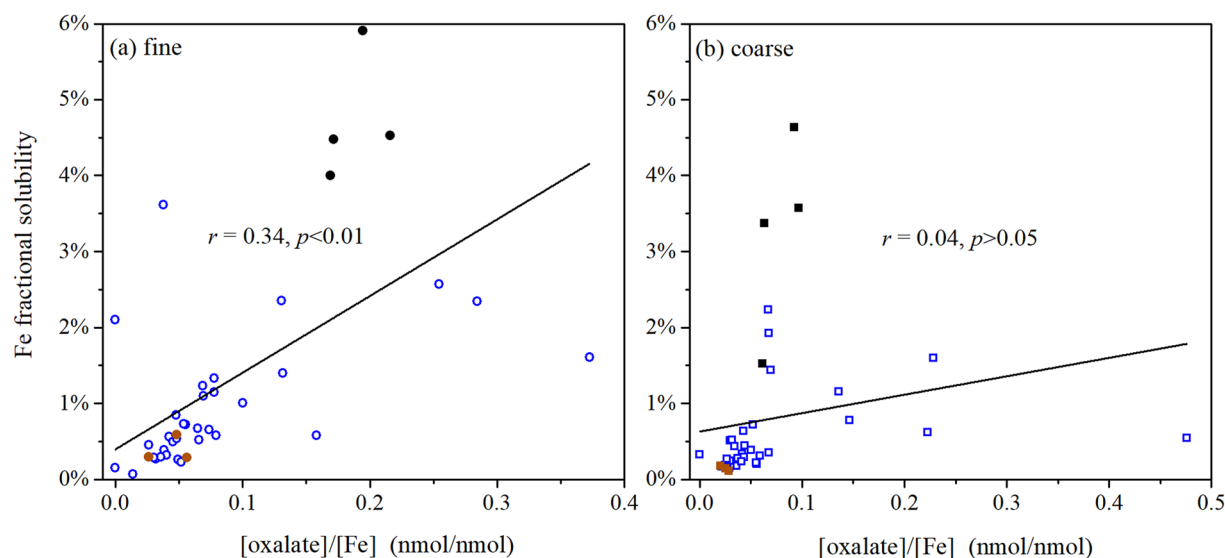
Figure 10. Fe solubility versus [oxalate]/[Fe]: (a) fine particles; (b) coarse particles. Dust days are represented by solid brown symbols, and haze days are represented by solid black symbols.

and Fe solubility for Saharan dust aerosol (Longo et al., 2016), and increase in aerosol acidity resulted in increase in Fe solubility for aerosol particles collected in Atlanta (Georgia, USA) (Fang et al., 2017). In addition, similar to what was found in our work, Fe solubility was lower when pH was >4 and significantly higher when pH < 4 for aerosol particles collected at five different sites over the globe (Ingall et al., 2018)

However, aerosol acidity was not the only factor which determined Fe solubility (Figure 9): when aerosol pH was lower than 4, Fe solubility could be either higher or lower than 1%. Figure 9 further reveals the importance of RH at higher aerosol acidity (pH < 4): Fe solubility was usually >1% when RH was >60% and <1% when RH was <60% for fine particles, although there were some outliers; furthermore, this trend was even more evident for coarse particles. In addition, Figure 9 shows that aerosol acidity and RH were both higher on haze days (higher Fe solubility) and both lower on dust days (lower Fe solubility).

The importance of RH in aerosol Fe solubility was also suggested by a few previous studies. For example, Zhu et al. (2020) collected aerosol particles during winter at four cities in eastern China, and found that Fe solubility was low (0.7%–3.8%) at <50% RH even though some samples had high values of $(2 \times [SO_4^{2-}] + [NO_3^-])/[Fe]$ (Zhu et al., 2020) and significantly higher (1.3%–11.4%) at >50% RH. In another study, Shi et al. (2020) found that for similar $(2 \times [SO_4^{2-}] + [NO_3^-])/[Fe]$ values, Fe solubility was much higher during fog days when average RH was 85%, compared to haze days. Overall, our work suggested that aerosol acidity and RH (thus aerosol water content) both play critical roles in regulating Fe solubility.

4.3. Effects of Organic Ligands

Laboratory studies (Chen & Grassian, 2013; Paris & Desboeufs, 2013; Wang et al., 2017) showed that the presence of organic ligands would promote Fe dissolution and thus increase Fe solubility. Figure 10 plots Fe solubility versus [oxalate]/[Fe] (the molar ratio of oxalate to Fe) for fine and coarse particles, and oxalate was chosen because it is likely the most abundant organic ligand in atmospheric aerosols and clouds. As shown in Figure 10, Fe solubility was reasonably well correlated with [oxalate]/[Fe] for fine particles, but there was no such correlation for coarse particles. This probably indicates that organic ligands may enhance Fe solubility in fine particles to some extent, but their effect on Fe solubility was not significant for coarse particles.

A very limited number of field measurements (Buck et al., 2006; Gao et al., 2019; Shi et al., 2020) explored the effects of organic ligands on aerosol Fe solubility, and the results appears to be contradictory. Compared to aerosol particles collected in the south of 80°N over the Arctic, both Fe solubility and relative contribution of carboxylates to total water-soluble ions were higher for aerosol particles collected in the north of 80°N (Gao et al., 2019), possibly indicating enhancement of aerosol Fe solubility by organic ligands; however, no obvious

correlation between Fe solubility and oxalate was observed for aerosol particles collected over the northwest Pacific (Buck et al., 2006) or aerosol particles collected in Qingdao (Shi et al., 2020). To summarize, it remains unclear whether organic ligands would significantly increase Fe solubility of ambient aerosol particles.

5. Summary and Conclusion

Fine (<1 μm) and coarse (>1 μm) particles were simultaneously collected during November–December 2019 at a suburban site in Qingdao, in order to understand abundance and fractional solubility of aerosol Fe. Average mass concentrations of total Fe were found to be 798 ± 466 and 801 ± 534 ng/m^3 for coarse (range: 195–2,193 ng/m^3) and fine particles (range: 104–2,301 ng/m^3) during the entire campaign, showing no significant difference between coarse and fine particles. Total Fe was well correlated with total Al for both fine and coarse particles, suggesting that desert dust was the major source for aerosol Fe. Furthermore, the median values of Fe enrichment factors were determined to be 2.6 and 1.9 for coarse and fine particles, implying nonnegligible contribution of non-dust sources to aerosol Fe. Average soluble Fe concentrations were found to be 7.7 ± 14.5 and 7.3 ± 7.6 for coarse (range: 0.6–73.7 ng/m^3) and fine particles (range: 0.6–41.2 ng/m^3), showing no significant difference between fine and coarse particles.

Fe solubility was found to be in the range of 0.11%–4.63% (average: 0.80 ± 1.03%) for coarse particles, significantly lower than those for fine particles (range: 0.07%–5.91%; average: 1.29 ± 1.41%). Higher Fe solubility in fine particles was partly because enhancement of Fe solubility by acid processing was more significant in fine particles, and this was supported by the fact that calculated pH values were lower for fine particles than coarse particles. It could also be partly due to enrichment of dust particles with lower Fe solubility in coarse particles and enrichment of anthropogenic particles with higher Fe solubility in fine particles.

When compared to clean days, total Fe concentrations were substantially increased during dust and haze days, and mass fractions of total Fe were elevated in dust days and reduced in haze days; moreover, soluble Fe concentrations showed no obvious change in dust day but were significantly increased during haze days, and Fe solubility was significantly reduced in dust days and enhanced during haze days. This implied that at least for our measurement periods, dust events did not lead to significant increase in soluble aerosol Fe though they substantially increase total aerosol Fe. Furthermore, Fe solubility in fine and coarse particles observed in our work during dust days was very similar to those for desert dust collected at source regions, indicating that Fe solubility of dust particles was not significantly increased when they were transported to Qingdao during dust events.

Fe solubility was correlated with BC, [nss-K$^+$]/[Al] and [Pb]/[Al] for fine particles, but such correlations did not exist or were very weak for coarse particles. This may imply that contribution of primary emission to Fe solubility enhancement was important for fine particles but minor for coarse particles. Fe solubility was well correlated relative abundance of secondary acidic species for both fine and coarse particles, indicating that acid processing significantly enhanced aerosol Fe solubility for coarse and fine particles. Our work found that higher Fe solubility (>1%) usually required high aerosol acidity (pH < 4) and high RH (>60%), revealing critical roles of aerosol acidity and water content in regulating aerosol Fe solubility.

Conflict of Interest

The authors declare no conflicts of interest relevant to this study.

Data Availability Statement

Data supporting this paper can be found at https://doi.org/10.5281/zenodo.5774638.

References

Alexander, B., Park, R. J., Jacob, D. J., & Gong, S. L. (2009). Transition metal-catalyzed oxidation of atmospheric sulfur: Global implications for the sulfur budget. *Journal of Geophysical Research*, *114*, 02310. https://doi.org/10.1029/2008jd010486

Baker, A. R., & Croot, P. L. (2010). Atmospheric and marine controls on aerosol iron solubility in seawater. *Marine Chemistry*, *120*, 4–13. https://doi.org/10.1016/j.marchem.2008.09.003

Baker, A. R., French, M., & Linge, K. L. (2006). Trends in aerosol nutrient solubility along a west–east transect of the Saharan dust plume. *Geophysical Research Letters*, *33*, L07805. https://doi.org/10.1029/2005gl024764

Baker, A. R., & Jickells, T. D. (2006). Mineral particle size as a control on aerosol iron solubility. *Geophysical Research Letters*, *33*, L17608. https://doi.org/10.1029/2006gl026557

Baker, A. R., Jickells, T. D., Witt, M., & Linge, K. L. (2006). Trends in the solubility of iron, aluminium, manganese and phosphorus in aerosol collected over the Atlantic Ocean. *Marine Chemistry*, *98*(1), 43–58. https://doi.org/10.1016/j.marchem.2005.06.004

Baker, A. R., Kanakidou, M., Nenes, A., Myriokefalitakis, S., Croot, P. L., Duce, R. A., et al. (2021). Changing atmospheric acidity as a modulator of nutrient deposition and ocean biogeochemistry. *Science Advances*, *7*. https://doi.org/10.1126/sciadv.abd8800

Baker, A. R., Li, M. P., & Chance, R. (2020). Trace metal fractional solubility in size-segregated aerosols from the tropical eastern Atlantic Ocean. *Global Biogeochemical Cycles*, *34*, e2019GB00651006510. https://doi.org/10.1029/2019gb006510

Boyd, P. W., & Ellwood, M. J. (2010). The biogeochemical cycle of iron in the ocean. *Nature Geoscience*, *3*, 675–682. https://doi.org/10.1038/ngeo964

Boyd, P. W., Jickells, T., Law, C. S., Blain, S., Boyle, E. A., Buesseler, K. O., et al. (2007). Mesoscale iron enrichment experiments 1993-2005: Synthesis and future directions. *Science*, *315*, 612–617. https://doi.org/10.1126/science.1131669

Buck, C. S., Landing, W. M., & Resing, J. A. (2010). Particle size and aerosol iron solubility: A high-resolution analysis of Atlantic aerosols. *Marine Chemistry*, *120*, 14–24. https://doi.org/10.1016/j.marchem.2008.11.002

Buck, C. S., Landing, W. M., Resing, J. A., & Lebon, G. T. (2006). Aerosol iron and aluminum solubility in the northwest Pacific Ocean: Results from the 2002 IOC cruise. *Geochemistry, Geophysics, Geosystems*, *7*, Q04M07. https://doi.org/10.1029/2005GC000977

Buck, C. S., Landing, W. M., Resing, J. A., & Measures, C. I. (2010). The solubility and deposition of aerosol Fe and other trace elements in the North Atlantic Ocean: Observations from the A16N CLIVAR/CO2 repeat hydrography section. *Marine Chemistry*, *120*, 57–70. https://doi.org/10.1016/j.marchem.2008.08.003

Cao, J. J., Chow, J. C., Watson, J. G., Wu, F., Han, Y. M., Jin, Z. D., et al. (2008). Size-differentiated source profiles for fugitive dust in the Chinese Loess Plateau. *Atmospheric Environment*, *42*, 2261–2275. https://doi.org/10.1016/j.atmosenv.2007.12.041

Chen, H. H., & Grassian, V. H. (2013). Iron dissolution of dust source materials during simulated acidic processing: The effect of sulfuric, acetic, and oxalic acids. *Environmental Science & Technology*, *47*, 10312–10321. https://doi.org/10.1021/es401285s

Chen, Y., & Siefert, R. L. (2004). Seasonal and spatial distributions and dry deposition fluxes of atmospheric total and labile iron over the tropical and subtropical North Atlantic Ocean. *Journal of Geophysical Research*, *109*, D09305. https://doi.org/10.1029/2003jd003958

Chuang, P. Y., Duvall, R. M., Shafer, M. M., & Schauer, J. J. (2005). The origin of water soluble particulate iron in the Asian atmospheric outflow. *Geophysical Research Letters*, *32*, L07813. https://doi.org/10.1029/2004gl021946

Conway, T. M., Hamilton, D. S., Shelley, R. U., Aguilar-Islas, A. M., Landing, W. M., Mahowald, N. M., & John, S. G. (2019). Tracing and constraining anthropogenic aerosol iron fluxes to the North Atlantic Ocean using iron isotopes. *Nature Communications*, *10*, 2628. https://doi.org/10.1038/s41467-019-10457-w

Conway, T. M., & John, S. G. (2014). Quantification of dissolved iron sources to the north Atlantic Ocean. *Nature*, *511*, 212–215. https://doi.org/10.1038/nature13482

Cui, S., Xian, J., Shen, F., Zhang, L., Deng, B., Zhang, Y., & Ge, X. (2021). One-year real-time measurement of black carbon in the rural area of Qingdao, northeastern China: Seasonal variations, meteorological effects, and the COVID-19 case analysis. *Atmosphere*, *12*, 394. https://doi.org/10.3390/atmos12030394

Cwiertny, D. M., Baltrusaitis, J., Hunter, G. J., Laskin, A., Scherer, M. M., & Grassian, V. H. (2008). Characterization and acid-mobilization study of iron-containing mineral dust source materials. *Journal of Geophysical Research*, *113*, D05202. https://doi.org/10.1029/2007jd009332

Daellenbach, K. R., Uzu, G., Jiang, J. H., Cassagnes, L. E., Leni, Z., Vlachou, A., et al. (2020). Sources of particulate-matter air pollution and its oxidative potential in Europe. *Nature*, *587*, 414–419. https://doi.org/10.1038/s41586-020-2902-8

Fang, T., Guo, H. Y., Zeng, L. H., Verma, V., Nenes, A., & Weber, R. J. (2017). Highly acidic ambient particles, soluble metals, and oxidative potential: A link between sulfate and aerosol toxicity. *Environmental Science & Technology*, *51*, 2611–2620. https://doi.org/10.1021/acs.est.6b06151

Fountoukis, C., & Nenes, A. (2007). ISORROPIA II: A computationally efficient thermodynamic equilibrium model for K^+-Ca^{2+}-Mg^{2+}-NH_4^+-Na^+-SO_4^{2-}-NO_3^--Cl^--H_2O aerosols. *Atmospheric Chemistry and Physics*, *7*, 4639–4659. https://doi.org/10.5194/acp-7-4639-2007

Fu, H. B., Shang, G. F., Lin, J., Hu, Y. J., Hu, Q. Q., Guo, L., et al. (2014). Fractional iron solubility of aerosol particles enhanced by biomass burning and ship emission in Shanghai, East China. *The Science of the Total Environment*, *481*, 377–391. https://doi.org/10.1016/j.scitotenv.2014.01.118

Fu, X., Guo, H., Wang, X., Ding, X., He, Q., Liu, T., & Zhang, Z. (2015). PM2.5 acidity at a background site in the Pearl River Delta region in fall-winter of 2007–2012. *Journal of Hazardous Materials*, *286*, 484–492. https://doi.org/10.1016/j.jhazmat.2015.01.022

Fu, X. X., Wang, X. M., Guo, H., Cheung, K. L., Ding, X., Zhao, X. Y., et al. (2014). Trends of ambient fine particles and major chemical components in the Pearl River Delta region: Observation at a regional background site in fall and winter. *The Science of the Total Environment*, *497*, 274–281. https://doi.org/10.1016/j.scitotenv.2014.08.008

Gao, Y., Marsay, C. M., Yu, S., Fan, S. Y., Mukherjee, P., Buck, C. S., & Landing, W. M. (2019). Particle-size variability of aerosol iron and impact on iron solubility and dry deposition fluxes to the Arctic Ocean. *Scientific Reports*, *9*, 16653. https://doi.org/10.1038/s41598-019-52468-z

Gao, Y., Xu, G., Zhan, J., Zhang, J., Li, W., Lin, Q., et al. (2013). Spatial and particle size distributions of atmospheric dissolvable iron in aerosols and its input to the Southern Ocean and coastal East Antarctica. *Journal of Geophysical Research*, *118*(12), 12634–12648. https://doi.org/10.1002/2013jd020367

Gao, Y., Yu, S., Sherrell, R. M., Fan, S., Bu, K., & Anderson, J. R. (2020). Particle-size distributions and solubility of aerosol iron over the Antarctic Peninsula during austral summer. *Journal of Geophysical Research: Atmospheres*, *125*, e2019JD032082032010. https://doi.org/10.1029/2019jd032082

Guieu, C., Bonnet, S., Wagener, T., & Loÿe-Pilot, M.-D. (2005). Biomass burning as a source of dissolved iron to the open ocean? *Geophysical Research Letters*, *32*, L19608. https://doi.org/10.1029/2005gl022962

Guo, H., Xu, L., Bougiatioti, A., Cerully, K. M., Capps, S. L., Hite, J. R., Jr, et al. (2015). Fine-particle water and pH in the southeastern United States. *Atmospheric Chemistry and Physics*, *15*, 5211–5228. https://doi.org/10.5194/acp-15-5211-2015

Hennigan, C. J., Izumi, J., Sullivan, A. P., Weber, R. J., & Nenes, A. (2015). A critical evaluation of proxy methods used to estimate the acidity of atmospheric particles. *Atmospheric Chemistry and Physics*, *15*, 2775–2790. https://doi.org/10.5194/acp-15-2775-2015

Hsu, S.-C., Lin, F.-J., & Jeng, W.-L. (2005). Seawater solubility of natural and anthropogenic metals within ambient aerosols collected from Taiwan coastal sites. *Atmospheric Environment*, *39*, 3989–4001. https://doi.org/10.1016/j.atmosenv.2005.03.033

Hsu, S.-C., Wong, G. T. F., Gong, G.-C., Shiah, F.-K., Huang, Y.-T., Kao, S.-J., et al. (2010). Sources, solubility, and dry deposition of aerosol trace elements over the East China Sea. *Marine Chemistry*, *120*, 116–127. https://doi.org/10.1016/j.marchem.2008.10.003

Ingall, E. D., Feng, Y., Longo, A. F., Lai, B., Shelley, R. U., Landing, W. M., et al. (2018). Enhanced iron solubility at low pH in global aerosols. *Atmosphere*, *9*, 201. https://doi.org/10.3390/atmos9050201

Ito, A. (2013). Global modeling study of potentially bioavailable iron input from shipboard aerosol sources to the ocean. *Global Biogeochemical Cycles*, *27*, 1–10. https://doi.org/10.1029/2012gb004378

Ito, A. (2015). Atmospheric processing of combustion aerosols as a source of bioavailable iron. *Environmental Science and Technology Letters*, *2*, 70–75. https://doi.org/10.1021/acs.estlett.5b00007

Ito, A., & Feng, Y. (2010). Role of dust alkalinity in acid mobilization of iron. *Atmospheric Chemistry and Physics*, *10*, 9237–9250. https://doi.org/10.5194/acp-10-9237-2010

Ito, A., Myriokefalitakis, S., Kanakidou, M., Mahowald, N. M., Scanza, R. A., Hamilton, D. S., et al. (2019). Pyrogenic iron: The missing link to high iron solubility in aerosols. *Science Advances*, *5*, eaau7671. https://doi.org/10.1126/sciadv.aau7671

Ito, A., & Shi, Z. (2016). Delivery of anthropogenic bioavailable iron from mineral dust and combustion aerosols to the ocean. *Atmospheric Chemistry and Physics*, *16*, 85–99. https://doi.org/10.5194/acp-16-85-2016

Ito, A., Ye, Y., Baldo, C., & Shi, Z. B. (2021). Ocean fertilization by pyrogenic aerosol iron. *npj Climate and Atmospheric Science*, *4*, 30. https://doi.org/10.1038/s41612-021-00185-8

Jickells, T., Boyd, P., & Hunter, K. A. (2014). Biogeochemical impacts of dust on the global carbon cycle. In P. Knippertz, & J.-B. W. Stuut (Eds.), *Mineral dust: A key player in the Earth system* (pp. 359–384). Springer Netherlands. https://doi.org/10.1007/978-94-017-8978-3_14

Jickells, T. D., An, Z. S., Andersen, K. K., Baker, A. R., Bergametti, G., Brooks, N., et al. (2005). Global iron connections between desert dust, ocean biogeochemistry, and climate. *Science*, *308*, 67–71. https://doi.org/10.1126/science.1105959

Johansen, A. M., & Hoffmann, M. R. (2003). Chemical characterization of ambient aerosol collected during the northeast monsoon season over the Arabian Sea: Labile-Fe(II) and other trace metals. *Journal of Geophysical Research*, *108*, 4408. https://doi.org/10.1029/2002jd003280

Kakavas, S., Patoulias, D., Zakoura, M., Nenes, A., & Pandis, S. N. (2021). Size-resolved aerosol pH over Europe during summer. *Atmospheric Chemistry and Physics*, *21*, 799–811. https://doi.org/10.5194/acp-21-799-2021

Kumar, A., & Sarin, M. M. (2010). Aerosol iron solubility in a semi-arid region: Temporal trend and impact of anthropogenic sources. *Tellus B: Chemical and Physical Meteorology*, *62*, 125–132. https://doi.org/10.1111/j.1600-0889.2009.00448.x

Kumar, A., Sarin, M. M., & Srinivas, B. (2010). Aerosol iron solubility over Bay of Bengal: Role of anthropogenic sources and chemical processing. *Marine Chemistry*, *121*, 167–175. https://doi.org/10.1016/j.marchem.2010.04.005

Li, W. J., Xu, L., Liu, X. H., Zhang, J. C., Lin, Y. T., Yao, X. H., et al. (2017). Air pollution–aerosol interactions produce more bioavailable iron for ocean ecosystems. *Science Advances*, *3*, e1601749. https://doi.org/10.1126/sciadv.1601749

Liu, L., Lin, Q., Liang, Z., Du, R., Zhang, G., Zhu, Y., et al. (2021). Variations in concentration and solubility of iron in atmospheric fine particles during the COVID-19 pandemic: An example from China. *Gondwana Research*, *97*, 138–144. https://doi.org/10.1016/j.gr.2021.05.022

Liu, M., Song, Y., Zhou, T., Xu, Z., Yan, C., Zheng, M., et al. (2017). Fine particle pH during severe haze episodes in northern China. *Geophysical Research Letters*, *44*, 5213–5221. https://doi.org/10.1002/2017gl073210

Longo, A. F., Feng, Y., Lai, B., Landing, W. M., Shelley, R. U., Nenes, A., et al. (2016). Influence of atmospheric processes on the solubility and composition of iron in Saharan dust. *Environmental Science & Technology*, *50*, 6912–6920. https://doi.org/10.1021/acs.est.6b02605

Luo, C., Mahowald, N., Bond, T., Chuang, P. Y., Artaxo, P., Siefert, R., et al. (2008). Combustion iron distribution and deposition. *Global Biogeochemical Cycles*, *22*, GB1012. https://doi.org/10.1029/2007GB002964

Luo, C., Mahowald, N. M., Meskhidze, N., Chen, Y., Siefert, R. L., Baker, A. R., & Johansen, A. M. (2005). Estimation of iron solubility from observations and a global aerosol model. *Journal of Geophysical Research*, *110*, D23307. https://doi.org/10.1029/2005jd006059

Mahowald, N. M., Baker, A. R., Bergametti, G., Brooks, N., Duce, R. A., Jickells, T. D., et al. (2005). Atmospheric global dust cycle and iron inputs to the ocean. *Global Biogeochemical Cycles*, *19*, GB4025. https://doi.org/10.1029/2004GB002402

Mahowald, N. M., Hamilton, D. S., Mackey, K. R. M., Moore, J. K., Baker, A. R., Scanza, R. A., & Zhang, Y. (2018). Aerosol trace metal leaching and impacts on marine microorganisms. *Nature Communications*, *9*, 2614. https://doi.org/10.1038/s41467-018-04970-7

Martin, J. H. (1990). Glacial-interglacial CO_2 change: The iron hypothesis. *Paleoceanography*, *5*, 1–13. https://doi.org/10.1029/pa005i001p00001

Martin, L. R., & Good, T. W. (1991). Catalyzed oxidation of sulfur dioxide in solution: The iron-manganese synergism. *Atmospheric Environment*, *25A*, 2395–2399. https://doi.org/10.1016/0960-1686(91)90113-l

McLennan, S. M. (2001). Relationships between the trace element composition of sedimentary rocks and upper continental crust. *Geochemistry, Geophysics, Geosystems*, *2*, 2000GC000109. https://doi.org/10.1029/2000gc000109

Meskhidze, N., Chameides, W. L., Nenes, A., & Chen, G. (2003). Iron mobilization in mineral dust: Can anthropogenic SO_2 emissions affect ocean productivity? *Geophysical Research Letters*, *30*, 2085. https://doi.org/10.1029/2003GL018035

Meskhidze, N., Volker, C., Al-Abadleh, H. A., Barbeau, K., Bressac, M., Buck, C., et al. (2019). Perspective on identifying and characterizing the processes controlling iron speciation and residence time at the atmosphere-ocean interface. *Marine Chemistry*, *217*, 103704. https://doi.org/10.1016/j.marchem.2019.103704

Moore, C. M., Mills, M. M., Arrigo, K. R., Berman-Frank, I., Bopp, L., Boyd, P. W., et al. (2013). Processes and patterns of oceanic nutrient limitation. *Nature Geoscience*, *6*, 701–710. https://doi.org/10.1038/ngeo1765

Morton, P. L., Landing, W. M., Hsu, S.-C., Milne, A., Aguilar-Islas, A. M., Baker, A. R., et al. (2013). Methods for the sampling and analysis of marine aerosols: Results from the 2008 GEOTRACES aerosol intercalibration experiment. *Limnology and Oceanography: Methods*, *11*, 62–78. https://doi.org/10.4319/lom.2013.11.62

Myriokefalitakis, S., Daskalakis, N., Mihalopoulos, N., Baker, A. R., Nenes, A., & Kanakidou, M. (2015). Changes in dissolved iron deposition to the oceans driven by human activity: A 3-D global modelling study. *Biogeosciences*, *12*, 3973–3992. https://doi.org/10.5194/bg-12-3973-2015

Myriokefalitakis, S., Ito, A., Kanakidou, M., Nenes, A., Krol, M. C., Mahowald, N. M., et al. (2018). Reviews and syntheses: The GESAMP atmospheric iron deposition model intercomparison study. *Biogeosciences*, *15*, 6659–6684. https://doi.org/10.5194/bg-15-6659-2018

Oakes, M., Ingall, E. D., Lai, B., Shafer, M. M., Hays, M. D., Liu, Z. G., et al. (2012). Iron solubility related to particle sulfur content in source emission and ambient fine particles. *Environmental Science & Technology*, *46*, 6637–6644. https://doi.org/10.1021/es300701c

Oakes, M., Weber, R. J., Lai, B., Russell, A., & Ingall, E. D. (2012). Characterization of iron speciation in urban and rural single particles using XANES spectroscopy and micro X-ray fluorescence measurements: Investigating the relationship between speciation and fractional iron solubility. *Atmospheric Chemistry and Physics*, *12*, 745–756. https://doi.org/10.5194/acp-12-745-2012

Ooki, A., Nishioka, J., Ono, T., & Noriki, S. (2009). Size dependence of iron solubility of Asian mineral dust particles. *Journal of Geophysical Research*, *114*, D03202. https://doi.org/10.1029/2008jd010804

Pant, P., & Harrison, R. M. (2012). Critical review of receptor modelling for particulate matter: A case study of India. *Atmospheric Environment*, *49*, 1–12. https://doi.org/10.1016/j.atmosenv.2011.11.060

Paris, R., & Desboeufs, K. V. (2013). Effect of atmospheric organic complexation on iron-bearing dust solubility. *Atmospheric Chemistry and Physics*, *13*, 4895–4905. https://doi.org/10.5194/acp-13-4895-2013

Paris, R., Desboeufs, K. V., Formenti, P., Nava, S., & Chou, C. (2010). Chemical characterisation of iron in dust and biomass burning aerosols during AMMA-SOP0/DABEX: Implication for iron solubility. *Atmospheric Chemistry and Physics*, *10*, 4273–4282. https://doi.org/10.5194/acp-10-4273-2010

Paris, R., Desboeufs, K. V., & Journet, E. (2011). Variability of dust iron solubility in atmospheric waters: Investigation of the role of oxalate organic complexation. *Atmospheric Environment*, *45*, 6510–6517. https://doi.org/10.1016/j.atmosenv.2011.08.068

Piel, C., Weller, R., Huke, M., & Wagenbach, D. (2006). Atmospheric methane sulfonate and non-sea-salt sulfate records at the European Project for Ice Coring in Antarctica (EPICA) deep-drilling site in Dronning Maud Land, Antarctica. *Journal of Geophysical Research*, *111*, D03304. https://doi.org/10.1029/2005jd006213

Scanza, R. A., Hamilton, D. S., Perez Garcia-Pando, C., Buck, C., Baker, A., & Mahowald, N. M. (2018). Atmospheric processing of iron in mineral and combustion aerosols: Development of an intermediate-complexity mechanism suitable for Earth system models. *Atmospheric Chemistry and Physics*, *18*, 14175–14196. https://doi.org/10.5194/acp-18-14175-2018

Schroth, A. W., Crusius, J., Sholkovitz, E. R., & Bostick, B. C. (2009). Iron solubility driven by speciation in dust sources to the ocean. *Nature Geoscience*, *2*, 337–340. https://doi.org/10.1038/ngeo501

Sedwick, P. N., Sholkovitz, E. R., & Church, T. M. (2007). Impact of anthropogenic combustion emissions on the fractional solubility of aerosol iron: Evidence from the Sargasso Sea. *Geochemistry, Geophysics, Geosystems*, *81*, Q10Q06. https://doi.org/10.1029/2007GC001586

Seinfeld, J. H., & Pandis, S. N. (2016). *Atmospheric chemistry and physics: From air pollution to climate change* (3rd ed.). Wiley Interscience.

Shelley, R. U., Landing, W. M., Ussher, S. J., Planquette, H., & Sarthou, G. (2018). Regional trends in the fractional solubility of Fe and other metals from North Atlantic aerosols (GEOTRACES cruises GA01 and GA03) following a two-stage leach. *Biogeosciences*, *15*, 2271–2288. https://doi.org/10.5194/bg-15-2271-2018

Shi, J. H., Guan, Y., Ito, A., Gao, H. W., Yao, X. H., Baker, A. R., & Zhang, D. Z. (2020). High production of soluble iron promoted by aerosol acidification in fog. *Geophysical Research Letters*, *47*, e2019GL086124. https://doi.org/10.1029/2019gl086124

Shi, Z., Bonneville, S., Krom, M. D., Carslaw, K. S., Jickells, T. D., Baker, A. R., & Benning, L. G. (2011). Iron dissolution kinetics of mineral dust at low pH during simulated atmospheric processing. *Atmospheric Chemistry and Physics*, *11*, 995–1007. https://doi.org/10.5194/acp-11-995-2011

Shi, Z., Krom, M. D., Bonneville, S., & Benning, L. G. (2015). Atmospheric processing outside clouds increases soluble iron in mineral dust. *Environmental Science & Technology*, *49*, 1472–1477. https://doi.org/10.1021/es504623x

Shi, Z. B., Krom, M. D., Jickells, T. D., Bonneville, S., Carslaw, K. S., Mihalopoulos, N., et al. (2012). Impacts on iron solubility in the mineral dust by processes in the source region and the atmosphere: A review. *Aeolian Research*, *5*, 21–42. https://doi.org/10.1016/j.aeolia.2012.03.001

Shi, Z. B., Woodhouse, M. T., Carslaw, K. S., Krom, M. D., Mann, G. W., Baker, A. R., et al. (2011). Minor effect of physical size sorting on iron solubility of transported mineral dust. *Atmospheric Chemistry and Physics*, *11*, 8459–8469. https://doi.org/10.5194/acp-11-8459-2011

Sholkovitz, E. R., Sedwick, P. N., & Church, T. M. (2009). Influence of anthropogenic combustion emissions on the deposition of soluble aerosol iron to the ocean: Empirical estimates for island sites in the North Atlantic. *Geochimica et Cosmochimica Acta*, *73*, 3981–4003. https://doi.org/10.1016/j.gca.2009.04.029

Sholkovitz, E. R., Sedwick, P. N., Church, T. M., Baker, A. R., & Powell, C. F. (2012). Fractional solubility of aerosol iron: Synthesis of a global-scale data set. *Geochimica et Cosmochimica Acta*, *89*, 173–189. https://doi.org/10.1016/j.gca.2012.04.022

Siefert, R. L., Johansen, A. M., & Hoffmann, M. R. (1999). Chemical characterization of ambient aerosol collected during the southwest monsoon and intermonsoon seasons over the Arabian Sea: Labile-Fe(II) and other trace metals. *Journal of Geophysical Research: Atmospheres*, *104*, 3511–3526. https://doi.org/10.1029/1998jd100067

Solmon, F., Chuang, P. Y., Meskhidze, N., & Chen, Y. (2009). Acidic processing of mineral dust iron by anthropogenic compounds over the north Pacific Ocean. *Journal of Geophysical Research: Atmospheres*, *114*, D02305. https://doi.org/10.1029/2008jd010417

Tagliabue, A., Bowie, A. R., Boyd, P. W., Buck, K. N., Johnson, K. S., & Saito, M. A. (2017). The integral role of iron in ocean biogeochemistry. *Nature*, *543*, 51–59. https://doi.org/10.1038/nature21058

Takahashi, Y., Furukawa, T., Kanai, Y., Uematsu, M., Zheng, G., & Marcus, M. A. (2013). Seasonal changes in Fe species and soluble Fe concentration in the atmosphere in the Northwest Pacific region based on the analysis of aerosols collected in Tsukuba, Japan. *Atmospheric Chemistry and Physics*, *13*, 7695–7710. https://doi.org/10.5194/acp-13-7695-2013

Tang, W., Llort, J., Weis, J., Perron, M. M. G., Basart, S., Li, Z., et al. (2021). Widespread phytoplankton blooms triggered by 2019–2020 Australian wildfires. *Nature*, *597*, 370–375. https://doi.org/10.1038/s41586-021-03805-8

Taylor, S. R., & McLennan, S. M. (1995). The geochemical evolution of the continental crust. *Reviews of Geophysics*, *33*, 241–265. https://doi.org/10.1029/95rg00262

Viana, M., Kuhlbusch, T. A. J., Querol, X., Alastuey, A., Harrison, R. M., Hopke, P. K., et al. (2008). Source apportionment of particulate matter in Europe: A review of methods and results. *Journal of Aerosol Science*, *39*, 827–849. https://doi.org/10.1016/j.jaerosci.2008.05.007

Wang, Y., Zhao, Y., Wang, Y., Yu, J. Z., Shao, J., Liu, P., et al. (2021). Organosulfates in atmospheric aerosols in Shanghai, China: Seasonal and interannual variability, origin, and formation mechanisms. *Atmospheric Chemistry and Physics*, *21*, 2959–2980. https://doi.org/10.5194/acp-21-2959-2021

Wang, Z., Fu, H., Zhang, L., Song, W., & Chen, J. (2017). Ligand-promoted photoreductive dissolution of goethite by atmospheric low-molecular dicarboxylates. *Journal of Physical Chemistry A*, *121*, 1647–1656. https://doi.org/10.1021/acs.jpca.6b09160

Wang, Z., Li, R., Cui, L., Fu, H., Lin, J., & Chen, J. (2018). Characterization and acid-mobilization study for typical iron-bearing clay mineral. *Journal of Environmental Sciences*, *71*, 222–232. https://doi.org/10.1016/j.jes.2018.04.012

Wiersma, G. B., & Davidson, C. I. (1986). Trace metals in the atmosphere of rural and remote areas. In J. Nriagu, & C. Davidson (Eds.), *Toxic metals in the atmosphere* (pp. 201–266). John Wiley.

Winton, V. H. L., Bowie, A. R., Edwards, R., Keywood, M., Townsend, A. T., van der Merwe, P., & Bollhofer, A. (2015). Fractional iron solubility of atmospheric iron inputs to the Southern Ocean. *Marine Chemistry*, *177*, 20–32. https://doi.org/10.1016/j.marchem.2015.06.006

Zhang, R., Cao, J. J., Tang, Y. R., Arimoto, R., Shen, Z. X., Wu, F., et al. (2014). Elemental profiles and signatures of fugitive dusts from Chinese deserts. *The Science of the Total Environment*, *472*, 1121–1129. https://doi.org/10.1016/j.scitotenv.2013.11.011

Zhang, T. R., Shi, J. H., Gao, H. W., Zhang, J., & Yao, X. H. (2013). Impact of source and atmospheric processing on Fe solubility in aerosols over the Yellow Sea, China. *Atmospheric Environment*, *75*, 249–256. https://doi.org/10.1016/j.atmosenv.2013.04.021

Zhu, Y. H., Li, W. J., Lin, Q. H., Yuan, Q., Liu, L., Zhang, J., et al. (2020). Iron solubility in fine particles associated with secondary acidic aerosols in east China. *Environmental Pollution*, *264*, 114769. https://doi.org/10.1016/j.envpol.2020.114769

AGU PUBLICATIONS

1

Supporting Information for

[Abundance and fractional solubility of aerosol iron during winter at a coastal city in northern China: similarities and contrasts between fine and coarse particles]

[Huanhuan Zhang,[1,2,6,a] Rui Li,[1,2,a] Shuwei Dong,[1] Fu Wang,[3] Yujiao Zhu,[4] He Meng,[5] Chengpeng Huang,[3] Yan Ren,[3] Xinfeng Wang,[4] Xiaodong Hu,[1] Tingting Li,[1] Chao Peng,[1] Guohua Zhang,[1] Likun Xue,[4] Xinming Wang,[1] Mingjin Tang,[1,2,6,*]]

[[1] State Key Laboratory of Organic Geochemistry, Guangdong Key Laboratory of Environmental Protection and Resources Utilization, and Guangdong-Hong Kong-Macao Joint Laboratory for Environmental Pollution and Control, Guangzhou Institute of Geochemistry, Chinese Academy of Sciences, Guangzhou, China

[2] CAS Center for Excellence in Deep Earth Science, Guangzhou, China

[3] Longhua Center for Disease Control and Prevention of Shenzhen, Shenzhen, China

[4] Environment Research Institute, Shandong University, Qingdao, China

[5] Qingdao Eco-environment Monitoring Center of Shandong Province, Qingdao, China

[6] University of Chinese Academy of Sciences, Beijing, China]

Contents of this file

Introduction

The supporting information contains one table and seven figures in total.

- Table S1 summarizes mass concentrations of different species ($PM_{2.5}$, PM_{10}, total Fe, soluble Fe, sulfate, nitrate, and ammonium) and Fe solubility during dust, haze and clean days.

- Figure S1 shows the wind rose during the campaign.

- Figure S2 shows time series of water soluble inorganic ions in fine and coarse particles, ratios of mass concentrations in fine particles to those in coarse particles for sulfate, nitrate and ammonium, and mass concentrations of black carbon.

- Figure S3 shows Fe solubility versus [nss-sulfate]/[Fe] and [nitrate]/[Fe] for fine and coarse particles.

- Figure S4 shows Fe solubility versus ($2\times$[sulfate]+[nitrate]) for fine and coarse particles.

- Figure S5 shows Fe solubility versus nss-sulfate and nitrate for fine and coarse particles.

- Figure S6 shows time series of mass concentrations of $PM_{2.5}$, PM_{10} and fine and coarse particles.

- Figure S7 shows Fe solubility versus BC concentrations, [nss-K^+]/[Al] and [Pb]/[Al] for coarse particles.

46 **Table S1.** Mass concentrations of $PM_{2.5}$ and PM_{10} ($\mu g/m^3$); total Fe concentration (ng/m^3), soluble

47 Fe concentration (ng/m^3) and Fe solubility (%) in fine and coarse particles; sulfate, nitrate, and

48 ammonium concentrations ($\mu g/m^3$) in fine and coarse particles during dust, haze and clean days.

49 The average values and standard deviations are provided.

|	dust days	haze days	clean days
$PM_{2.5}$	43±10	170±49	22±10
PM_{10}	118±14	215±57	35±7
total Fe in fine particle	1601±635	480±160	329±203
total Fe in coarse particle	1605±538	1252±367	285±63
soluble Fe in fine particle	6.1±2.8	23.7±12.3	6.3±8.1
soluble Fe in coarse particle	2.4±1.3	41.2±23.7	1.7±1.3
Fe solubility in fine particle	0.39±0.17	4.73±0.82	1.75±1.33
Fe solubility in coarse particle	0.14±0.03	3.28±1.29	0.61±0.39
sulfate in fine particle	2.5±0.6	8.3±1.9	2.0±0.8
sulfate in coarse particle	1.2±0.7	11.1±6.2	1.2±0.6
nitrate in fine particle	4.0±2.5	13.7±2.9	0.9±0.4
nitrate in coarse particle	2.9±3.6	16.2±4.4	1.5±1.0
ammonium in fine particle	2.6±1.1	9.0±1.5	1.4±0.4
ammonium in coarse particle	1.2±1.0	11.3±4.9	0.9±0.4

50

51

52

53

54

55
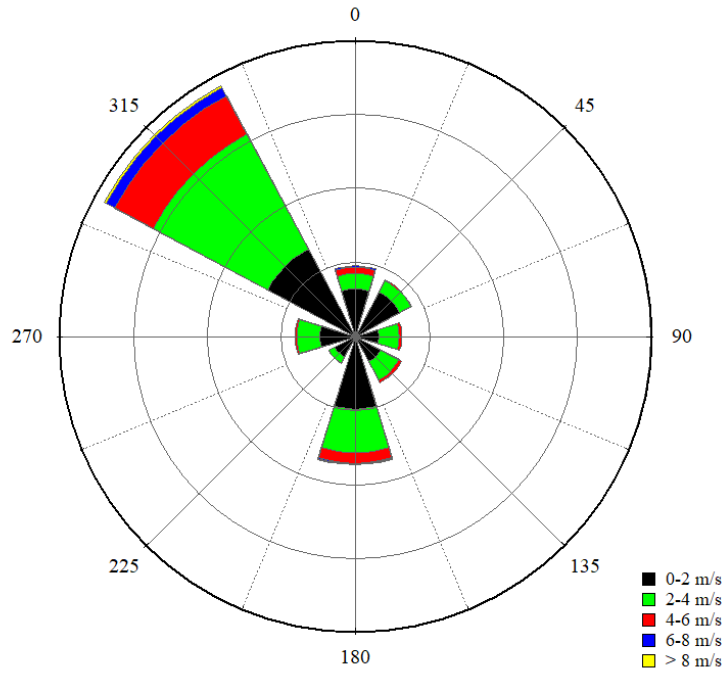
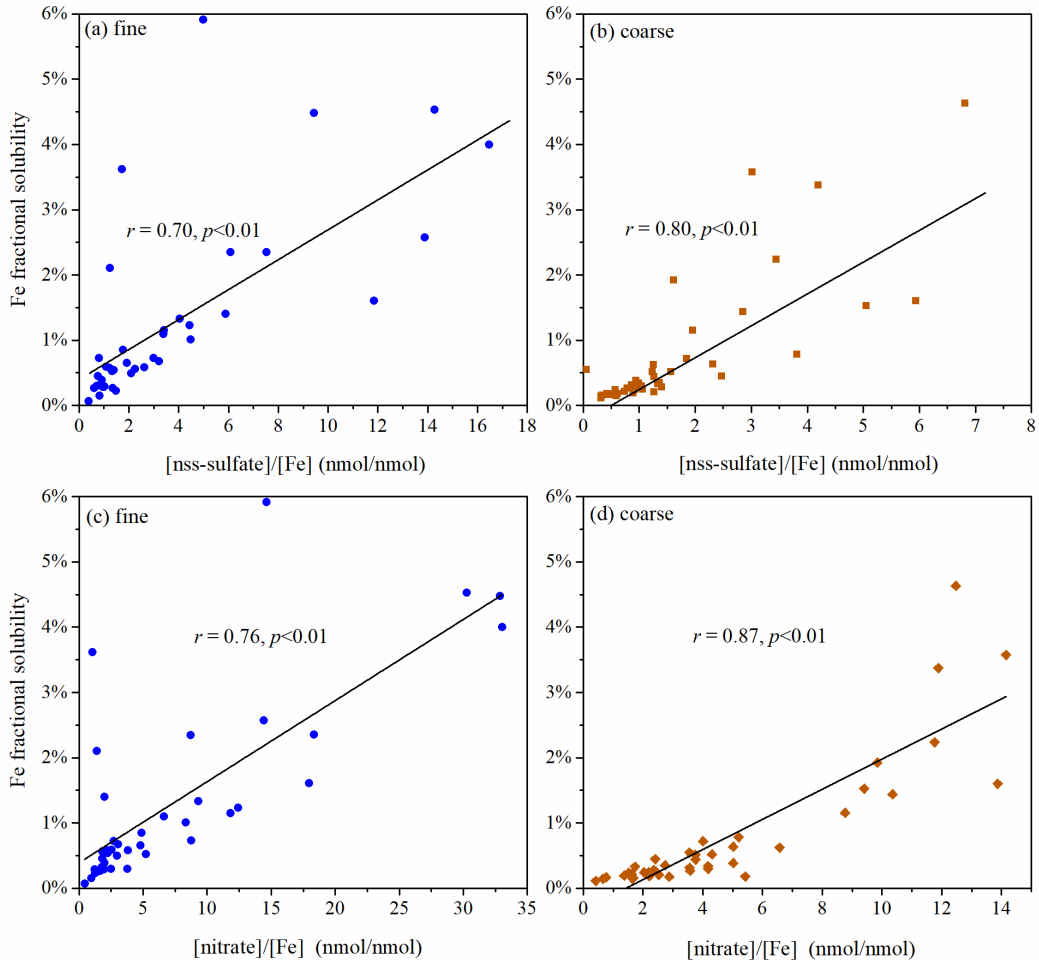**Figure S1.** Wind rose which displays wind directions and speeds during the campaign.

56

57

58

59

60
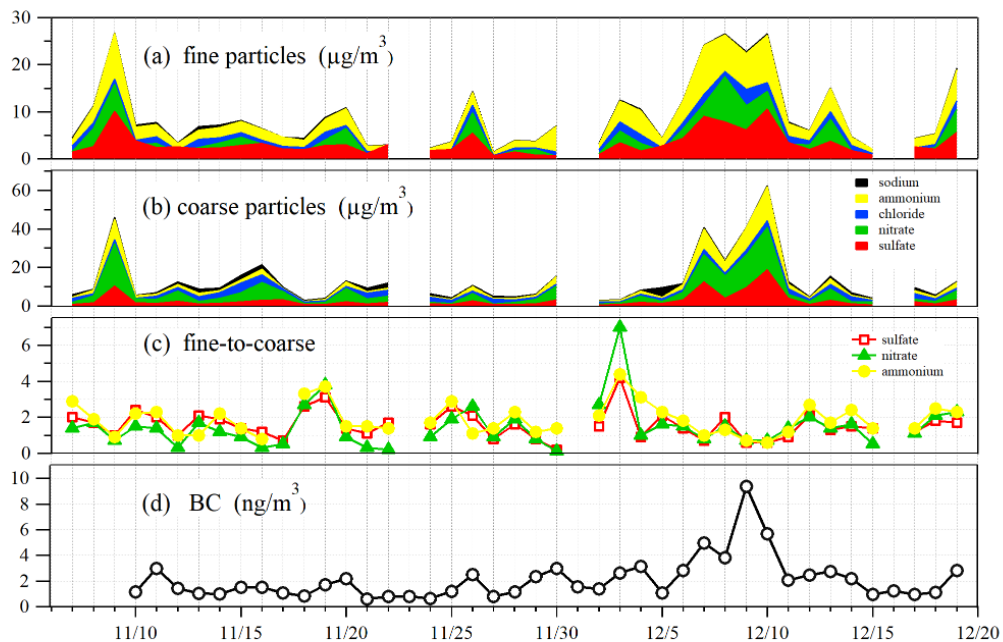
Figure S2. Time series of (a) water soluble inorganic ions in fine particles, (b) water soluble inorganic ions in coarse particles, (c) ratios of mass concentrations in fine particles to those in coarse particles for sulfate, nitrate and ammonium, and (d) black carbon.
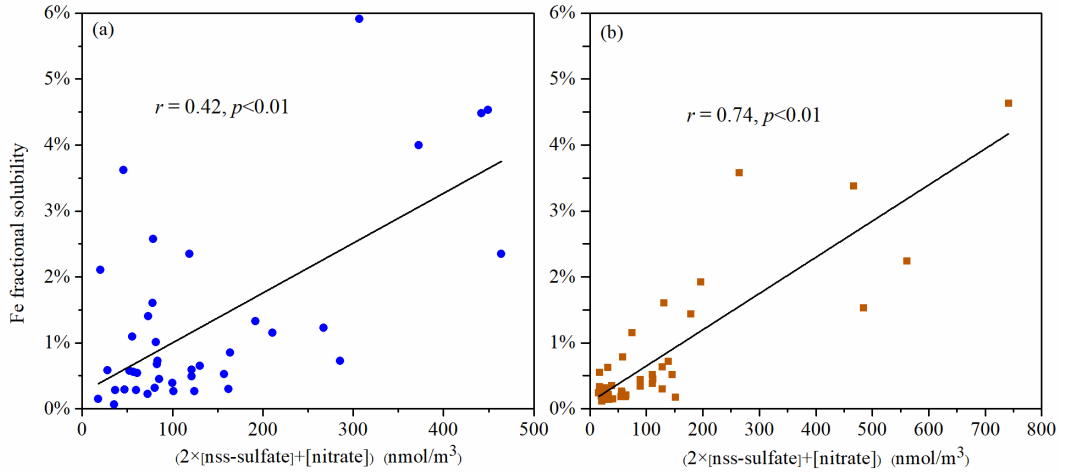
64

65

66

Figure S3. (a) Fe solubility versus [nss-sulfate]/[Fe] for fine particles; (b) Fe solubility versus [nss-sulfate]/[Fe] for coarse particles; (c) Fe solubility versus [nitrate]/[Fe] for fine particles; (d) Fe solubility versus [nitrate]/[Fe] for coarse particles.
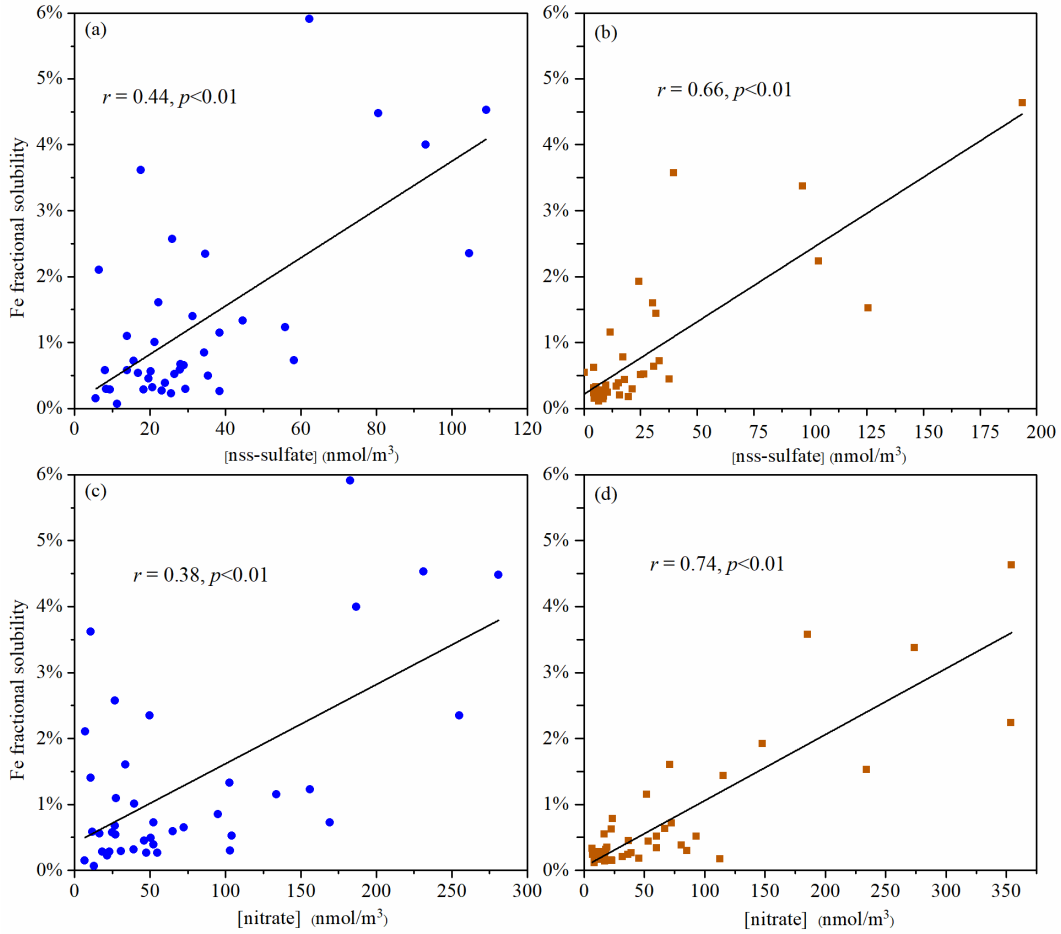
74

Figure S4. Fe solubility versus (2×[sulfate]+[nitrate]) (nmol/m^3): (a) fine particles; (b) coarse
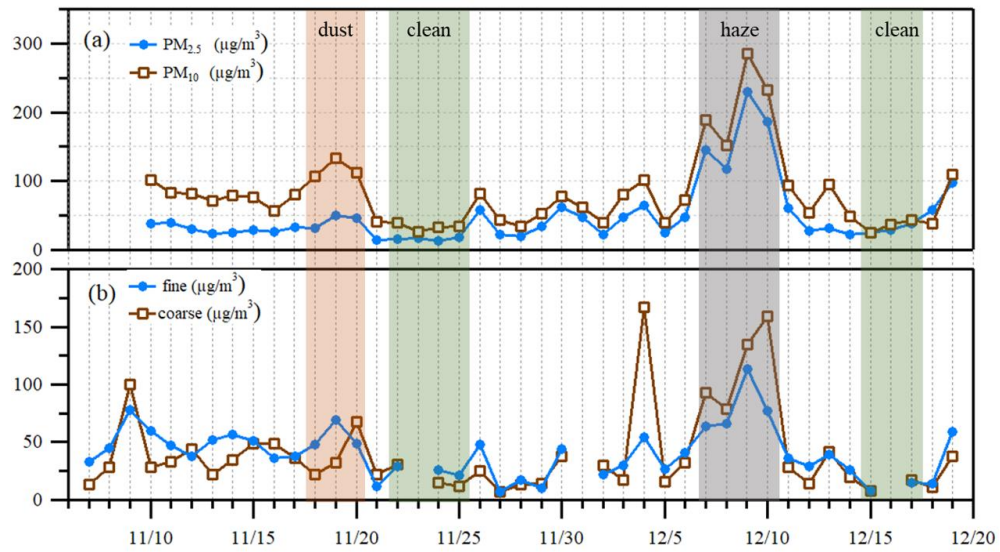
particles.

77

78

79

80

Figure S5. (a) Fe solubility versus nss-sulfate (nmol/m^3) for fine particles; (b) Fe solubility versus nss-sulfate (nmol/m^3) for coarse particles; (c) Fe solubility versus nitrate (nmol/m^3) for fine particles; (d) Fe solubility versus nitrate (nmol/m^3) for coarse particles.
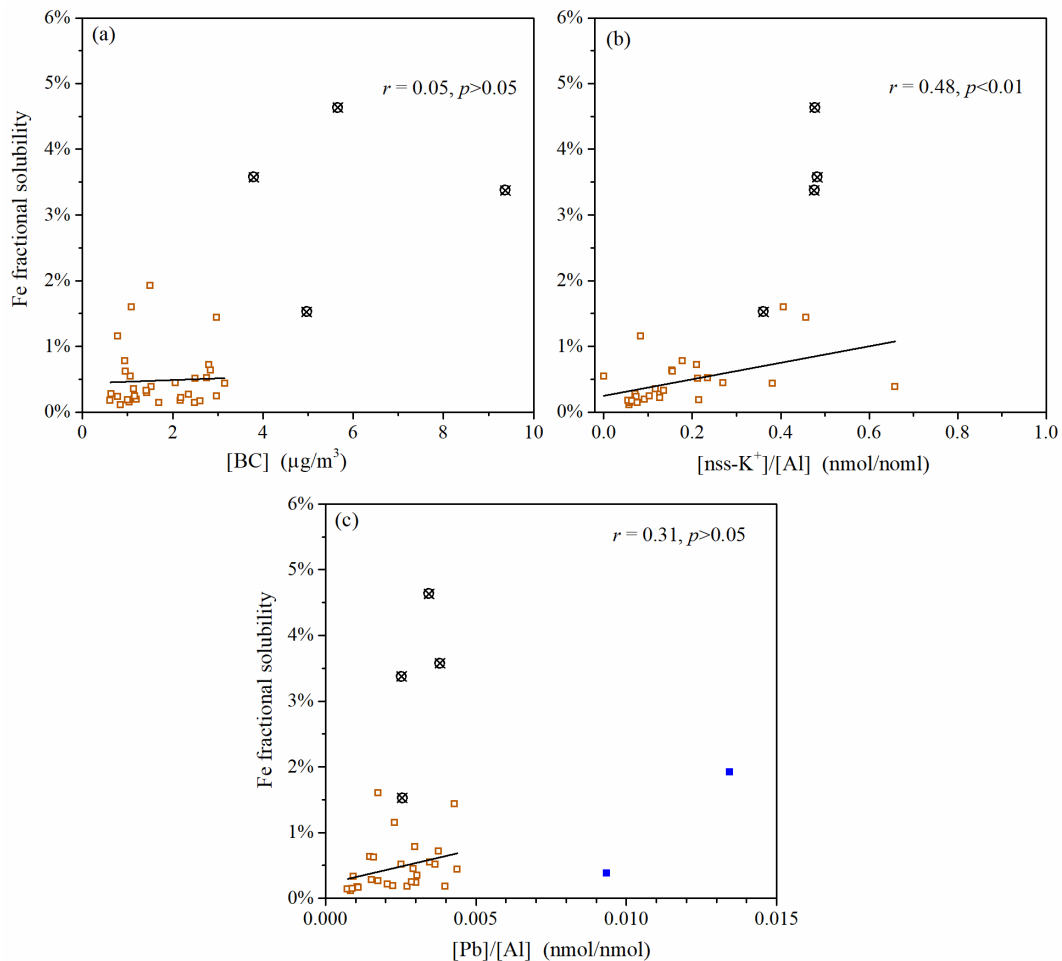
87

Figure S6. Time series of mass concentrations of aerosol particles: (a) $PM_{2.5}$ and PM_{10}; (b) fine

and coarse particles.

90

91

92

Figure S7. Fe solubility versus (a) BC concentrations, (b) [nss-K$^+$]/[Al] and (c) [Pb]/[Al] for coarse particles. Haze days, represented by black squares, are not included in correlation analysis; in addition, the two outliers, represented by blue squares in Figure S7c, are not included in correlation analysis.